Norwegian University of Life Sciences

Master's Thesis 2021 60 ECTS

Faculty of Environmental Sciences and Natual Resource Management

Long term biological effects of ionizing radiation on the eye development in γ-irradiated Atlantic salmon embryos

Oscar Mork

Chemistry and Biotechnology

Preface

This thesis is the final work of an integrated master program in Chemistry and Biotechnology, marking the end of my education at the Norwegian University of Life Sciences (NMBU). The project was a collaboration between the Center of Environmental Radioactivity (CERAD) and the Center of eye research at the Oslo University Hospital and was funded by both institutions. All experiments regarding exposure, rearing of fish, and sampling have been performed at NMBU from the autumn of 2015 and were finished in March 2016. Some of the sample preparation was done at the Plant-cell laboratory at NMBU (2021), but most of the laboratory work was performed at Ullevål during the spring of 2021.

First, I would like to thank my main supervisor Dr. Hans-Christian Teien and co-supervisor Dr. Dag Anders Brede for including me in this exciting project, for good guidance and interesting scientific discussions, and for giving valuable feedback on the final thesis. I would also like to thank Professor Goran Petrovski and Natasha Josifovska at the Center of Eye research for teaching me new techniques and guiding me through the laboratory work. I have learned a great deal from both of you and will be forever grateful for the time you took to supervise and participate in this project. Thank you, Professor emerita Brit Salbu for participating in discussions, for reading through my thesis and for giving valuable feedback. Also, I want to thank Prof. Erling Olaf Koppang for showing interest in my assignment and taking the time to help me with both laboratory techniques and interpretation of the results. Finally, I would also like to thank Tone Ingeborg Melby and Lene Cecilie Hermansen for your patience and flexibility, and for guiding me at the Plant-cell laboratory.

Lastly, I would like to thank everybody that have made my time as a student at NMBU some of the best years of my life. I really appreciate all the thousand cups of coffee and other beverages consumed during lazy hours or fiery debates and discussion. I would also like to thank my grandfather for being so supportive and always showing keen interest in my education, ever since my early days in primary school. That has meant a lot to me, and still does.

Oscar Mork

Ås, December 2021

Abstract

Organisms are at their most sensitive to ionizing radiation during the embryonic life stage, and the eye is one of the most sensitive tissues. High proliferation-rate, cell-differentiation and embryonic development depend on intact DNA and other biomolecules. In the present study, eyes of Atlantic salmon (*Salmo salar)* were studied at the stage of transition between alevin and fry, after a three-month recovery period from exposure to γ-radiation at dose-rates of 1, 10, and 20 mGy/h during the entire embryonic development. Long-term effects on development of eyes were assessed through histological methods, and molecular responses were investigated through immunofluorescence. In addition, effect of ionizing radiation on development of cataract was investigated by use of molecular marker responses. Whole eyes from non-irradiated salmon parr were also dissected and analyzed for documentation of potential effects associated with formalin fixation and its implications for histochemical analysis of eye-globes.

Histological analysis of heads from Salmon fry using 3.5 µm thick hematoxylin-eosin (HE) stained sections revealed no significant differences in tissue structure between exposed individuals and the control group, regardless of dose-rate. Extended storage on formalin did not have a negative effect on the outcome of HE-staining, and the tissue showed no apparent artefacts after dissection and dehydration. Prolonged fixation of salmon alevin did not impact the reactivity with immunofluorescent labels.

Molecular effects were investigated by staining 3.5 µm paraffin sections with primary antibodies and a rhodamine red fluorescent secondary antibody. Autophagy in the eye was investigated by labeling with microtubule associated protein 1 light chain 3 (LC3), but the marker revealed no significant effect from radiation.

Apoptosis and cell-proliferaion were investigated by labeling with Caspase-3, Ki-67 and Anti-Proliferating Cell Nuclear Antigen (PCNA) antibodies respectively, but none of the markers gave detectable levels, most likely due to incompatibility between the antibodies used and *Salmo salar* as a species.

Fibrosis was investigated using α-Smooth Muscle Actin (α-SMA), and despite no visible fibrotic tissue in the eye, elevated levels of the enzyme was found as a response to doses above 10 mGy/h.

Oxidative DNA damage was investigated by labeling with 8-hydroxy-2'-deoxyguanosine (8OHdG), 8-oxoguanine-DNA glycosylase (OGG1), Apurinic/apyrimidinic endonuclease 1 (APE1) and anti-DNA polymerase-β for detection of base excision repair (BER) activity. No persistent damage to nuclear DNA was found 3 months after exposure, although detection of cytoplasmic 8OHdG and APE1 suggests damage

to mRNA and mitochondrial DNA (mtDNA) independent of dose. Slightly elevated levels of DNA-pol β in the nuclei could be seen in irradiated fish in a dose-dependent manner.

Although clinical cataract was not directly assessed, mechanisms associated with developing cataracts were identified. Detection of markers for fibrotic tissue and oxidative damage in the lens and lens-epithelial cells (LECs) increased in a dose dependent manner after exposure to γ-radiation and may suggest a future development of cataracts.

Sammendrag

Organismer er på sitt mest sårbare for ioniserende stråling i det embryonale livsstadiet, og øyet er et av de mest sensitive organene. Høy celleproliferasjon, celledifferensiering og embryonal utvikling er avhengig av intakt DNA og andre biomolekyler. I det nåværende studiet ble øyer fra atlantisk laks (*Salmo salar)* studert ved overgangen fra plommesekkyngel til yngel, etter en tre måneders restitueringsperiode fra eksponering med γ-stråling ved doseratene 1, 10 og 20 mGy/h under den embryonale utviklingen. Langtidseffekter på utvikling av øyet ble vurdert gjennom histologiske metoder, og molekylære responser ble undersøkt gjennom immunfluorescens. I tillegg ble effekter knyttet til ioniserende stråling og utvikling av katarakt undersøkt ved bruk av molekylære markører. Hele øyne fra ikke-bestrålte lakse-parr ble også dissekert og undersøkt for dokumentasjon av mulige effekter forbundet med formalin-fiksering og implikasjonene for histokjemisk analyse av øye-globen.

Histologisk undersøkelse av hoder fra lakseyngel ved bruk av 3,5 µm tykke haematoxylin-eosine (HE) fargede snitt avslørte ingen signifikante forskjeller i vevsstrukturer mellom eksponerte individer og kontrollgruppen, uavhengig av doserate. Lang lagring på formalin hadde ingen negativ effekt på utfallet av HE-fargningen, og vevet viste ingen åpenbare artefakter etter disseksjon og dehydrering. Forlenget fiksering av lakseyngel hadde heller ingen effekt på reaktiviteten til immunfluoriserende markører.

Molekylære effekter ble undersøkt ved å farge 3,5 µm tykke parafinsnitt med primære antistoffer og et rhodamin-rødt fluoriserende sekundært antistoff. Autofagi i øyet ble undersøkt ved merking med mikrotubuli-assosiert protein lettkjede 3 (LC3), men markøren viste ingen signifikant effekt fra stråling.

Apoptose og celleproliferasjon ble undersøkt med henholdsvis caspase-3, Ki-67 og antiprolifererende nukleært antigen (PCNA), men ingen av markørene viste sporbare nivåer, mest sannsynlig et resultat av manglende kompatibilitet mellom antistoff og *Salmo salar* som art.

Fibrose ble undersøkt med α-glatt muskel aktin (α-SMA), og økte nivåer av enzymet ble funnet som et resultat av stråling til tross for at fibrose ikke ble observert.

Oksidativ DNA-skade ble undersøkt ved å merke prøvene med henholdsvis 8-hydroxy-2'-deoxyguanosie (8OHdG), 8-oxoguanin-DNA glykosylase (OGG1), Apurinisk/apyrimidinsk endonuklease 1 (APE1) og anti-DNA-polymerase β (DNA-pol β) for deteksjon av base-eksisjons-reparasjon (BER) aktivitet. Ingen persistent skade i nukleært DNA ble funnet 3 måneder etter eksponering, men deteksjon av cytoplasmisk 8OHdG og APE1 indikerer skade på mRNA og mitokondrielt DNA (mtDNA) uavhengig av stråledose.

Noe forhøyde nivåer av DNA-pol β i cellekjernen kunne observeres i et dose-avhengig forhold i eksponert fisk.

Selv om klinisk katarakt ikke ble vurdert direkte, ble mekanismer forbundet med utvikling av katarakt identifisert. Deteksjon av markører for fibrose og oksidativ skade i linsen og linses epitelceller (LECs) økte på en doseavhengig måte etter eksponering med γ-stråling, og kan indikere en fremtidig utvikling av katarakt.

List of abbreviations

APE1	Apurinic endonuclease 1
ARC	Age related cataract
BER	Base excision repair
8OHdG	8-hydroxy-2'-deoxyguoanosine
DBS	Double strand break
DNA-pol β	DNA Polymerase Beta
EMT	Epithelial mesenchymal transition
GI	Genomic instability
HE	Hematoxylin and Eosin
LC3	Microtubule associated protein light chain 3
LEC	Lens epithelial cells
LET	Linear energy transfer
LNT	Linear no-threshold model
mtDNA	Mitochondrial DNA
OFZ	Organelle free zone
OGG1	Oxoguanine DNA glycosylase 1
PBS	Phosphate buffered saline
PCNA	Proliferating cell nuclear antigen
PSC	Posterior subcapsular cataract
ROS	Reactive oxygen species
RPE	Retinal pigment epithelium
SSB	Single strand break
α-SMA	Alpha-Smooth Muscle Actin

Table of contents

1. Introduction

Ionizing radiation and associated biological effects have been a topic of interest and concern since the early days of discovery. Humans and other organisms are exposed to ionizing radiation originating from naturally occurring radioactive materials (NORM), or from anthropogenic sources such as fallout from nuclear weapons and fuel cycles. Following severe nuclear events, such as the Chernobyl accident, contamination have led to exposure and biological effects to both man and biota, especially in fish living in closed aquatic systems as seen in lakes within the Chernobyl region (Kaglyan et al., 2019, Teien et al., 2021).

Being long-ranged, γ-radiation is a key contributor to the external received dose and thus adverse biological effects caused by radioactive materials in the environment (UNSCEAR, 1993). Effects due to high doses (above 100 mGy) are well documented (deterministic effects such as radiation sickness and cataract), and the effect of acute exposure is well understood (Claycamp et al., 2000). However, the effects caused by chronic exposure and low dose radiation (stochastic effects) are far less investigated, and remain somewhat unclear (Shuryak, 2020, Boice et al., 2019).

Different developmental stages for living organisms have been proposed to be particularly sensitive to ionizing radiation, but finding specific thresholds for when different types of damages occurs remain unsuccessful (Barrett et al., 2018). Humans and other organisms such as fish are at their most vulnerable to ionizing radiation during early development of the embryo due to the high levels of cell divisions, proliferation rate and differentiation of stem cells (Hurem et al., 2017). As contaminated sediments are regarded as key contributors to the external dose (Lerebours et al., 2018), fish species such as the Atlantic salmon (*Salmo salar)*, who lay their eggs on the riverbed, are thus considered to receive high doses of radiation during the developmental stage.

Additionally, the extent of damages in living organisms due to low-dose radiation is highly dependent on the type of tissue being exposed. Besides the reproductive system, the eye and lens is considered one of the most radiosensitive of all organs (Hamada et al., 2020). Opacification of the lens, known as cataract, is suggested as an adverse outcome in humans from exposure to ionizing radiation, and is documented through different epidemiological studies after nuclear events such as the bombing of Hiroshima and Nagasaki, liquidators from the Chernobyl nuclear power plant clean up and workers at the Mayak nuclear facility (Ainsbury et al., 2016, Azizova et al., 2018). Although the relationship between exposure to ionizing radiation and cataract is evident in man, the mechanisms behind radiation induced cataractogenesis are not entirely understood. Experiments have been conducted *in vivo*, investigating the

effects of prenatal exposure to ionizing radiation on murine lenses, showing a relationship between dose and adverse outcome such as cataract also in smaller animals (Barnard et al., 2021, Barnard et al., 2019, Barnard et al., 2018, Dalke et al., 2018). A study from 2014 looked at the effects of X-rays on the development of eyes in zebrafish embryos, but found no obvious deleterious effects (Zhou et al., 2014). However, the embryos only received single-dose exposures at 8 hours post fertilization. Thus, the effects such as tissue damage, underdevelopment, or cataracts due to chronic exposure throughout the entire developmental stage were not assessed. Other studies have reported high incidence-rates of severe cataract in Atlantic salmon from fish farms in Norway, Scotland and Ireland (Wall, 1998), as well as in wild populations, and several probable explanatory mechanisms were proposed (Olsvik et al., 2020, Bjerkås et al., 2004, Remø et al., 2017). Nevertheless, none of these studies addressed the relationships between cataract and ionizing radiation.

The main objectives of the present study were to 1) assess the long-term biological effects of ionizing radiation on the eye development in γ-irradiated Atlantic salmon embryos; and 2) investigate a potential dose-response relationships between exposure and effects such as cataracts. To address histological changes and molecular effects related to tissue damage and cataract in irradiated Atlantic salmon, a series of endpoints were investigated in embryos exposed to different dose-rates of γ-radiation (1 mGy/h, 10 mGy/h and 20 mGy/h) during the entire developmental phase. The following hypotheses were tested:

H0: Chronic exposure to ionizing radiation during embryonic development leads to deformities and persistent eye damage

H1: Chronic exposure to ionizing radiation leads to cataract-associated responses

H2: Antibodies used for human immunolabeling may be used for investigation of cataract related responses in fish

2. Theory

2.1 Ionizing radiation

In the electromagnetic spectrum, ionizing radiation exists in the form of γ-photons or X-rays. Although γ-rays are electromagnetic waves, it differs from visible light in that the amount of energy carried by the photons is much larger. Upon interaction with matter, γ-radiation leaves a long track with low ionization density, thus depositing the energy over a large area. This property of energy deposition is referred to as the linear energy transfer (LET) (Choppin et al., 2014).

Gamma radiation is characterized as low-LET radiation, but the long range combined with an ability to penetrate matter makes it the main concern for damage due to external exposure (Kryshev and Sazykina, 2012). The ability to penetrate matter also implies that damage caused by γ-photons or X-rays is distributed throughout the entire organism in contrast to the non-electromagnetic ionizing radiation. As a result, protective shielding demands dense materials such as lead, concrete, or large bodies of water (Amirabadi et al., 2013).

The non-electromagnetic ionizing radiation consists of α –, β – , proton or neutron particles. As particles have a larger mass than photons, alpha- and beta – radiation carries more energy and has a higher LET than γ- or X-rays. More mass and larger size restricts range and ability to penetrate matter, but consequently will cause more damage per particle received compared to electromagnetic radiation (Choppin et al., 2014). However, due to the limited range, non-electromagnetic radiation remains hazardous mainly upon ingestion, inhalation or in close contact with tissue, although some radionuclides are known to accumulate in tissue and will thus contribute to the internal dose (Teien et al., 2021).

2.2 Biological effects of ionizing radiation

Biological effects caused by ionizing radiation are divided in different categories, namely direct-, indirect and non-targeted effects (Desouky et al., 2015). Whereas the direct effects are caused by the interaction between ionizing radiation and cellular structures, the indirect effects are caused by intermediate products such as free radical and reactive oxygen species (ROS). Non-targeted effects are damage seen in non-irradiated cells, known as bystander-cells, including inflammation and inflammatory responses, damage to DNA, or induction of other cellular stress responses (Al-Mayah et al., 2015, Morgan and Sowa, 2015, Azzam et al., 2012). These mechanisms are general and apply to different living organisms in addition to humans.

Furthermore, the biological effects caused by interaction with ionizing radiation are regarded as either deterministic or stochastic. Deterministic effects, or "tissue effects", are immediate and inevitable responses such as necrosis and tissue damage, formation of cataract, radiation sickness or even death (Ainsbury et al., 2016). This is mostly associated with high acute doses of radiation above a certain threshold following exposure from high-LET radiation such as α-particles, although deterministic effects may also arise from electromagnetic ionizing radiation. Stochastic effects, or probabilistic effects, concern outcome where the incidental risk increases with higher received doses, manifesting at a later stage in life (Hamada and Fujimichi, 2014). Cancer-development or persistent and heritable genetic damage are examples where probability of occurrence increases after exposure to ionizing radiation (Wakeford, 2004, Little et al., 2009). Effects occurring some time after irradiation, such as cancer, are referred to as late effects and are usually stochastic. These late effects are often related to unrepaired DNA damage causing genomic instability (GI), persistent damage to tissues or formation of cataracts, although cataract is regarded deterministic (Kamstra et al., 2018).

In aquatic populations, dose rates ranging from 2-10 mGy/day are recommended benchmark values at which no adverse effects are expected (Hurem et al., 2017). The dose-rates used in the present experiment were all within the derived consideration reference levels (DCRL) for fish (0.42 mGy/h – 40 mGy/h), where some observable adverse effects are expected (ICRP, 2012a). As the eye is particularly sensitive, observation of some adverse effects were expected, and mechanisms considered relevant regarding mitigation of damage in the eye are presented in the following chapters.

2.2.1 DNA damage

When ionizing radiation interacts directly with a DNA molecule, it may lead to single (SSB) or double strand breaks (DBS). High-LET radiation such as α-particles would cause a higher proportion of complex DNA damage compared to the lower-LET γ-radiation. Both interaction between ionizing radiation and water molecules, and mitochondrial respiration form free radicals (e.g. $H^{\bullet}$, $HO^{\bullet}$, and the recombinant H_2O_2) in the cell, which leads to the formation of a series of reactive oxygen species (ROS) (Riley, 1994, Liang and Godley, 2003). High concentrations of ROS may lead to oxidative stress or inflict oxidative lesions and mutations onto biomolecules such as DNA, and a well-functioning defense and repair system is crucial for cell viability (Havaki et al., 2015). If not properly mitigated, DNA-lesions may cause genomic instability (GI), which have been reported as a common effect after γ-radiation exposure in both fish and humans (Al-Mayah et al., 2015, Kadhim et al., 2013, Kamstra et al., 2018).

When a single DNA nucleotide is damaged, either as a direct or indirect effect from ionizing radiation, it must be replaced, and there are several different ways this can be achieved. Base excision repair (BER) is an important control mechanism that recognizes lesions in the DNA strand and ensures proper DNA-damage repair prior to replication (Krokan and Bjoras, 2013). Unrepaired DNA damage have previously been associated with eventual cataractogenesis (Ainsbury et al., 2016, Xu et al., 2015), and increased levels of the BER enzymes presented in the following chapters have been reported in the lens-epithelial-cells (LECs) of human patients with age-related cataracts (Xu et al., 2015).

During BER, the damaged base is excised from the DNA helix by a glycosylase before an endonuclease removes the remaining phosphate sugar, leaving a gap in the DNA strand. A DNA polymerase then fills the gap with a complimentary base before the strand is finally sealed by a ligase (Krokan and Bjoras, 2013). The human BER mechanism and guanosine-specific enzymes described in the following sections is illustrated in figure 2.1, but orthologs to these enzymes are also found in *Salmo salar*.

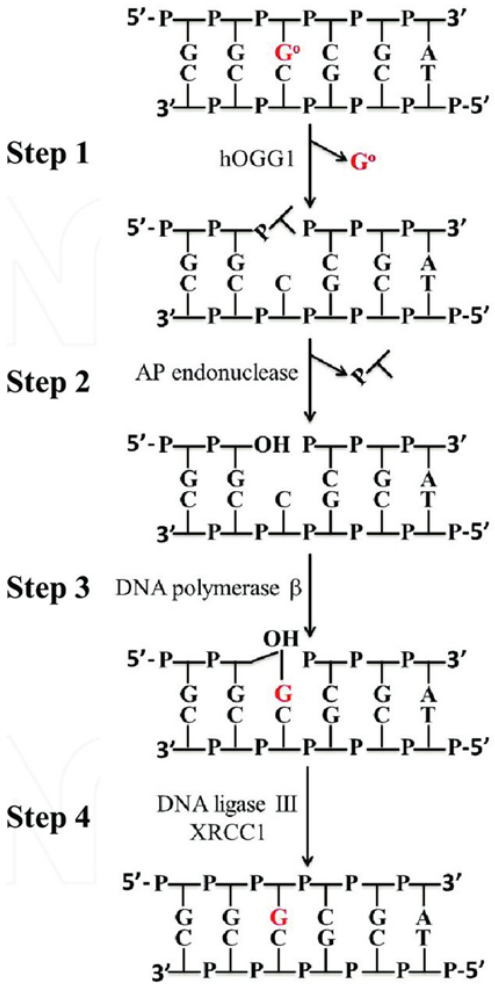

Figure 2.1 Base excision repair (BER) of an oxidized guanosine base (8OHdG) in a mammalian cell. Adopted from (Wu et al., 2017)

8-hydroxy,2-deoxyguanosie (8OHdG)

Of all DNA bases, guanosine is the most sensitive to oxidative damage. Due to its low redox potential, it is readily oxidized to the analog 8-hydroxy,2-deoxyguanosine (8OHdG), causing changes in its binding properties with the complementary cytosine base (Kino et al., 2017). This particular lesion, if not addressed by the DNA-repair system, may lead to G-T and C-A transition mutations during replication, which in turn may have detrimental effects on the organism (Cheng et al., 1992, Wang et al., 2018). Elevated levels of 8OHdG in the vitreous have been reported in patients suffering from diabetic retinopathy (Abdulhussein et al., 2021).

Oxoguanine glycosylase 1 (OGG1)

Oxoguanine glycosylase (OGG1) is an enzyme which primary function is to remove 8-hydroxy,2-deoxyguanosine (8OHdG) base lesions that are produced from interaction between ROS and the DNA molecules (step 1, figure 2.1). OGG1 scans the DNA strands for oxidative lesions on the guanine base with great precision and is the primary step in the BER pathway for this specific damage (Wang et al., 2018). The glycosylase acts by binding to the oxidized base, flipping it out of the helical structure before excising it, leaving an apurinic site in its place. An apurinic site refers only to the lack of a purine base, often referred to as an abasic site (Krokan and Bjoras, 2013).

Apurinic endonuclease 1 (APE1)

Prior to the insertion of a new nucleotide, the sugar-phosphate backbone from the damaged base left by OGG1 must be removed from the DNA-helix. Apurinic/apyrimidic endonuclease 1 (APE1) is a multifunctional protein, and one of the main properties is its endonuclease abilities (Tell et al., 2009). After OGG1 has removed the damaged base, the endonuclease is recruited to the apurinic site where it makes an incision in the sugar-phosphate backbone leaving an empty gap, prepared to receive a new nucleotide (step 3, figure 2.1).

In addition to its role in DNA-damage repair, APE1 is also involved in the repair of mRNA and mitochondrial DNA in response to oxidative stress (Barchiesi et al., 2021). Mitochondrial DNA accumulate high levels of 8OHdG due to the amount of ROS generated as a by-product from the electron transport chain. APE1 binding with RNA molecules is significantly increased by oxidative stress in the mitochondria (Barchiesi et al., 2021).

Furthermore, APE-1 may also serve as a post-transcriptional regulator of gene expression by degrading RNA (Thakur et al., 2014). Additionally, a redox potential is encoded in the N-terminal end of the

mammalian enzyme (Xanthoudakis et al., 1994). This property is completely independent from the repairing abilities that are localized in the C-region (Tell et al., 2009). The nuclear export signal is also found within the N-terminal region, but as this region is not as highly conserved, the redox properties have not been found in zebrafish and seems to apply only in mammalian species (Georgiadis et al., 2008).

DNA-Polymerase β (DNA-pol-β)

After removal of the damaged base from the DNA strand, DNA-polymerase β (DNA-pol-β) is recruited to insert a new and functional base, thus fulfilling the repair. DNA-pol-β is known as the smallest of the polymerase-enzymes, and is involved in nucleotide excision repair (NER), post replication mismatch- and DBS repair, in addition to BER (Beard and Wilson, 2014). Additionally, overexpression of the enzyme has been identified with cataractogenesis in young mice (Sobol, 2003)

2.2.2 Tissue damage and repair

Ionizing radiation may cause damage to lipids, membranes and other macromolecules of the cells, in addition to DNA-damage. When injury is inflicted on cells and tissue due to γ-radiation, several mechanisms may be induced to limit deleterious effects eventually leading to eye disease or loss of functionality. The mechanisms described in the following chapters are based on human biology, but apoptosis, autophagy and fibrosis have also been reported in fish after exposure to ionizing radiation (Epperly et al., 2012).

Apoptosis

Apoptosis is a cascade of events culminating in the disintegration of cells having sustained unmendable damage. As opposed to necrosis, which is an uncontrolled cell death, apoptosis is organized and a type of "programmed cell death". Several pathways are related to apoptosis, but mainly the intrinsic is associated with radiation exposure (Lauber et al., 2012, Elmore, 2007). Intramembrane proteins found within mitochondria are released to the cell cytoplasm, inducing the formation of a protein complex called the apoptosome, triggering a series of downstream events. Eventually, activation of the caspase-3 protein, which is associated with the execution pathway, leads to the final degradation of the cell (Elmore, 2007). Apoptosis is involved in eye-related diseases such as retinopathy and macular degradation (Abdulhussein et al., 2021), whilst its role in cataractogenesis, on the other hand, is highly debated, and studies have reported conflicting results (Harocopos et al., 1998, Li et al., 1995).

Autophagy

Autophagy is carried out by the immune system to clear damaged or dying cells during apoptosis, in addition to "daily maintenance" of the cell (Glick et al., 2010). When a cellular structure or organelle is damaged by ionizing radiation nor oxidative stress, certain mechanisms of mitigation are triggered in the organism. Studies have shown that autophagy is upregulated in response to ionizing radiation exposure and is often associated with controlled cell death. It is, however, not certain whether autophagy induces cell death or if cell death is a result of failed cell rescue and autophagy (Palumbo, 2013).

The autophagosome is an internal vacuole materializing from existing cellular membranes that folds and pinches off to form a single layer membrane bound vesicle. Due to its association with the autophagosome membrane, Microtubule-associated protein 1 light-chain 3 (LC3) is used as a marker for cell autophagy (Ito et al., 2005). Autophagosomes engulfs macromolecules marked for recycling, and after filling up the vesicle it merges with a lysosome, forming an auto(phago)lysosome as illustrated in Figure 2.2 (Ito et al., 2005). The lysosome is another membrane bound vesicle containing different lysosomal enzymes. These enzymes, known as hydrolases, degenerate and break down the inner membrane of the autophagosome and its contents before releasing them to the cell for re-use in other processes. In this manner, organelles that are damaged or broken are recycled into components that may be reused in construction and synthesis of new organelles and other molecules within the cell, revitalizing otherwise badly damaged cells (Chaurasia et al., 2016). In the differentiating cells of the lens, autophagy plays an important role in removal and degradation of organelles, contributing to lens clarity (Frost et al., 2014).

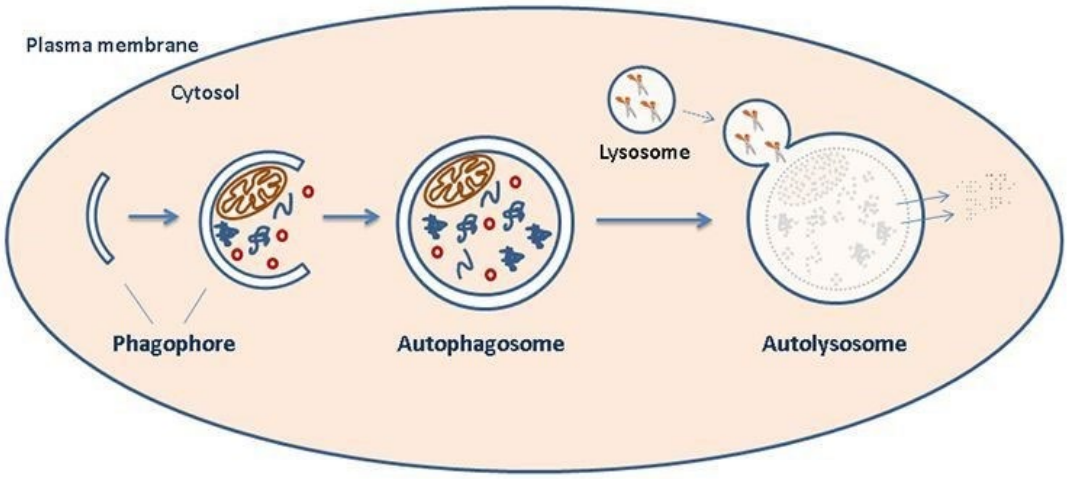

Figure 2.2 Illustration of the autophagy process. Adapted from https://www.creative-diagnostics.com/autophagy.htm

Fibrosis and Epithelial mesenchymal transition

After radiation therapy, fiber like cell-structures in patients have been documented (Judge et al., 2015), and the phenomenon is referred to as fibrosis. During fibrosis, tissue will form fiber like structures resembling what is seen during healing of mechanical wounds. The α Smooth Muscle Actin (α-SMA) is an actin protein, most commonly associated with the smooth muscle cells as the name implies. In general, this protein is important in the formation of myofibroblasts, which is the transition phase between fibroblast (cells that make up the connective tissue) and smooth muscle cells (Gabbiani, 1992).

It is also known as an important contributor to the epithelial-mesenchymal-transition (EMT), which is a process where epithelial cells become mobile and form mesenchymal fiber cells (Kalluri and Weinberg, 2009, Park et al., 2019). This type of fibrous structures has been documented as a cause of posterior capsular cataracts after cataract surgery in humans (Nagamoto et al., 2000, Hillenmayer et al., 2020).

2.2.3 Cataract formation

The eye, with its internal structures, is a very sensitive organ. When the lens is exposed to different types of stress, the clear fiber cells may become opacified resulting in reduced visibility (Berthoud and Beyer, 2009). Opacification of the lens is referred to as cataracts and there is as of today no effective treatment for it, except replacing it with an artificial one. Due to the lack of treatment, cataracts remain a severe problem as it is also one of the most common human eye-related diseases (Brian and Taylor, 2001).

Human cataract disease is divided in three types depending on their localization in the lens. Nuclear cataracts are caused by opacification in the center of the lens; cortical cataracts arise in the periphery (cortex) of the lens and stretches towards the center like rays; posterior-subcapsular cataracts (PSC) is found near the posterior pole and develop underneath the lens capsule (Ainsbury et al., 2016). Although nuclear- and cortical cataracts have the highest prevalence in a normal human population, PSC is the type of cataract most commonly associated with exposure to ionizing radiation (ICRP, 2012b).

PSC may develop as a result of chronic and low doses of radiation, but the actual threshold and dose-response relationship is still a topic of debate. Previous limits have been set at 2 Gy for acute exposure, and 5 Gy doses received in smaller fractions over a period of time (Ainsbury et al., 2016). These thresholds have more recently been lowered to a maximum dose of 0.5 Gy received by the eye (ICRP, 2012b). The exact mechanisms for formation of cataracts after exposure to ionizing radiation is still somewhat unclear, but the larger cohort studies of the Mayak workers and A-bomb survivors have contributed to the new dose regulations with respect to cataract (Azizova et al., 2018).

Different mechanisms have been associated with the formation of cataracts. A study regarding age related cataracts found elevated levels of BER enzymes in cells from patients with cataracts, but also formation of fibroblasts from LECs and rapid development of the eye have been associated with opacified lenses (Xu et al., 2015, Bjerkås et al., 1996). Although the above mentioned mechanisms are related to human cataract, several factors such as rapid growth, diet imbalance, water temperature and changes in water salinity have been documented to cause cataracts in farmed Atlantic salmon (Bjerkås et al., 1996, Bjerkås et al., 2004). In salmon, different types of irreversible cataracts are recognized, but additionally, reversible osmotic cataracts have been documented, especially during smoltification (Bjerkås et al., 2004).

2.2.4 Dose response from ionizing radiation

Considerable efforts have been devoted to the development of models describing the dose-response relationship on eye damage from low doses of ionizing radiation in human and through animal models such as mice (Dalke et al., 2018, Hamada, 2017, Barnard et al., 2019, Barnard et al., 2018). Although there is consensus regarding the general effects caused by high doses of ionizing radiation, the model most commonly used for predicting the outcome of low dose ionizing radiation, namely linear no-threshold model (LNT), is often debated (Lall et al., 2014). Some models suggest that low doses are in fact beneficial, and that harmful effects only occur when the dose exceeds a certain threshold (Joussen et al., 2001). Effects such as cataract may only manifest at a later stage following exposure and distinguishing between radiation induced effects and the general population incidence rate can be difficult. Large cohort studies are challenging, but historic events such as the atomic bomb survivors from Hiroshima and Nagasaki, workers at the Mayak nuclear installation and the Chernobyl liquidators have proven a valuable source of information. Results from such retrospective cohort studies strengthen the LNT model (Azizova et al., 2018, Little et al., 2009).

2.3 Atlantic salmon, *Salmo Salar,* as a model organism

Fish is known to be one of the most radiosensitive of all aquatic organisms, particularly at the embryonic stage (UNSCEAR, 2008). As some radionuclides are soluble in water, ingestion and exposure through the gills is a possible pathway for receiving an internal dose, but β- and γ-radiation from suspended radioactive particles may also contribute to external dose (UNSCEAR, 2008). Contamination associated with the sediments also impose a hazard to fish, as some species both spawn and feed from the sediments, and thus receive an external dose from γ and β radiation and internal dose through ingestion of radioactive particles and uptake through the gills (Lerebours et al., 2018). Due to its sensitivity and

importance in the ecosystem, fish is commonly used as a model organism in exposure studies (Kamstra et al., 2018, Lindeman et al., 2019, Song et al., 2012)

The Atlantic salmon, *Salmo Salar,* is often used in the Norwegian fish and aquaculture industry for production, making it an important model organism in two aspects. Firstly, rearing conditions have been optimized for fish growth and wellbeing, and secondly, knowledge regarding health effects due to environmental factors are important for further improvement of fish health.

In nature, Atlantic salmon spawns in the river sediments during spring. After spawning, the eggs swell in contact with water due to osmosis, absorbing potentially contaminated water. Consequently, fish embryos are exposed to radiation both from the sediments and from radioactive matter suspended in the waterbody during the entire developmental phase. As previously mentioned, the embryonic stage is also recognized as particularly sensitive to ionizing radiation (UNSCEAR, 2008, Mothersill et al., 2010).

Although the entire organism is of interest, the eye is particularly intriguing to investigate due to its complexity. As opposed to other organs, the eye consists of both regenerative tissue such as the retina, sustaining a continuous blood supply, and the lens which depends on aqueous and vitreous humor for nutrition and other essential compounds (Dahm et al., 2011). Studying the eye will show how different tissues respond to ionizing radiation based on the physical environment surrounding them, and how this affects the persistence of damage.

2.4 Embryonic development of the eye and lens in fish

Formation of the eye and lens starts early in the embryonic development. The eye capsule forms after gastrulation, during the somitogenesis, and consists of tissues that will later differentiate into the cornea, lens and retina (Gorodilov, 1996). Somitogenesis is a developmental stage recognized by the formation of mitotic and differentiated somite cells, making up specific tissues in the organism. In this phase, different parts of the developing organism are easily recognized. After somitogenesis, vascularization of the yolk-sac begins, and the eyes are covered by pigmentation making them visible through the egg-envelope (Gorodilov, 1996). This stage is referred to as “eyed egg” (Macqueen et al., 2008). A schematic overview of the developing eye cup is presented in figure 2.3.

The development of the eye and lens in fish is different from what is seen in mammals and birds (Kozłowski, 2018, Dahm et al., 2007). In mammals, after forming the eye capsule, the outer cell layer of the blastula known as the ectoderm, pinches off to form a hollow vesicle that will later fill with differentiated fiber cells and develop into a lens. In fish on the other hand, the lens develops from a solid

cluster of cells that is attached to the ectoderm layer (image A and B, figure 2.3). This cluster will grow and eventually separate before the anterior and posterior chamber of the eye is formed on either side of the premature lens (Dahm et al., 2007). Both chambers are filled with either aqueous or vitreous humor respectively, and the fluids contain growth factors that encourage differentiation of the epithelial cells encapsulating the lens (red cells seen in figure 2.4), separating the differentiated fiber cells from the internal environment of the eye. There is, however, no literature describing whether these differences affect the general susceptibility to cataract in fish compared with humans or other mammals.

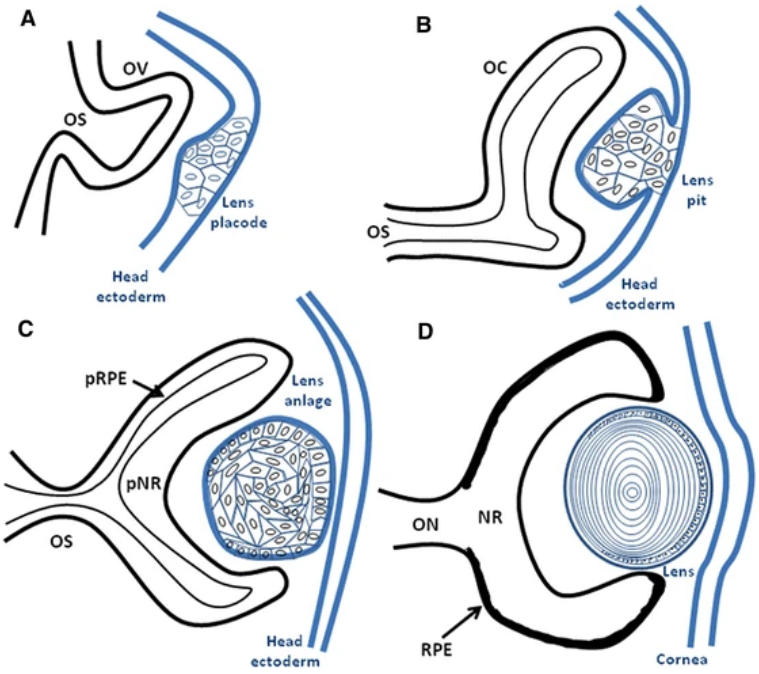

Figure 2.3 Schematic presentation of the embryonic eye development in fish. A) Formation of the optic vesicle. B) The cluster of cells eventually forming the lens can be seen in the ectoderm, and the optic vesicle is transitioning to an optic cup. C)The optic cup is developing to a retina, and the lens has separated from the ectoderm. D) Properly developed eye. Adapted from (Bejarano-Escobar et al., 2014)

2.4.1 Lens cell differentiation in fish

The anterior part of the lens is covered by a single layer of cells called the lens epithelial cells (LECs) (Bjerkås et al., 2004). These cells move along the surface of the lens from the anterior pole towards the posterior pole, differentiating to lens fiber cells along the way. To ensure a clear vision, the lens fiber cells must be free of organelles that may shatter and disperse the light. Consequently, the differentiating LECs are deprived of organelles such as the nucleus, mitochondria, and Golgi apparatus etc. After differentiation and removal of the large intracellular components, empty fiber cells continue their migration and build up the layers of the lens. This process is hugely important for lens clarity, and interruptions from radiation or other stressors may have a negative impact on the fulfillment and successful removal of organelles (Wride, 2011). In mammalian species, differentiation of the epithelial

cells take place near the equator of the lens. Fish LECs differentiate as they approach the posterior pole of the lens. As a result, cells containing nuclei, organelles and other macromolecules are found closer to the posterior pole of lenses from fish compared to mammals. This phenomenon is thought to help disperse the light in fish lenses more, contributing to a wider field of view.

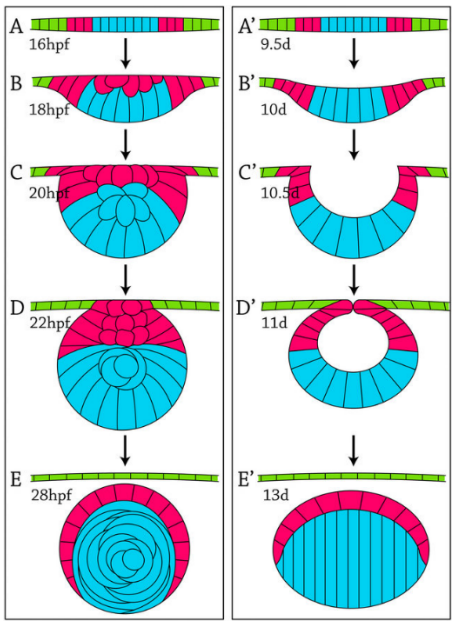

Figure 2.4 Cell Fate and Differentiation of the Developing Ocular Lens. The left column illustrates the differentiating lens of a zebrafish, while the right column illustrates a differentiating mammalian lens. Adapted from (Greiling et al., 2009).

Not only lens formation differs between mammals and fish. In most mammalian species, the lens has an oval shape as opposed to the spherical shape seen in fish (figure 2.4) . An explanation for this difference may be found by looking to the environment in which the organism is living. While the refraction index between water and the aqueous humor inside the cornea is almost identical, there is a great difference between air and the aqueous humor (Kozłowski, 2018). Difference in refraction index greatly impacts the way light focuses on the retina, as the transition between air and the aqueous humor naturally causes light to change direction when traveling from one material to the other. In fish, light enters the eye in an almost straight line due to the similar refractive indexes of water and aqueous humor. Fish vision is therefore entirely dependent on the refractive power of the lens to focus light on the retina (Dahm et al., 2007, Mahler et al., 2013).

Part of what gives lens fiber cells their refractive power are the crystalline proteins found in the cytoplasm. Due to the refractive requirements, a higher concentration of crystalline proteins is needed in lenses from fish compared to terrestrial animals, making piscine lenses more rigid than e.g. mammalian

(Zhao et al., 2014). This high concentration of proteins suggests a higher latency for cataract development due to cross linkage caused by both radiation, oxidative stress or other factors (Bjerkås et al., 2004). Lens fiber cells are never replaced, meaning that the ones found in the lens-nucleus are created in the early stages of development and will remain throughout the entire lifetime of the organism (Kozłowski, 2018). This implies that damage to the fiber cells and its protein contents is highly accumulative.

Exposure to radiation during the developmental stages may have detrimental effects to the individual (Barrett et al., 2018). Complex damage to the DNA and other important structures may delay the development severely, as cell division and differentiation is reliant on intact genetic material. Unpublished results from Teien et al. revealed severe underdevelopment of the eyes in salmon alevin (larvae) exposed to doses of 20 mGy/h during embryonal development, compared to individuals receiving lower doses and dose-rates (Figure 2.5). As illustrated in figure 2.6, increased levels of apoptotic markers were also found in the exposed samples in a dose dependent manner, showing how vulnerable fish embryos are to ionizing radiation during development.

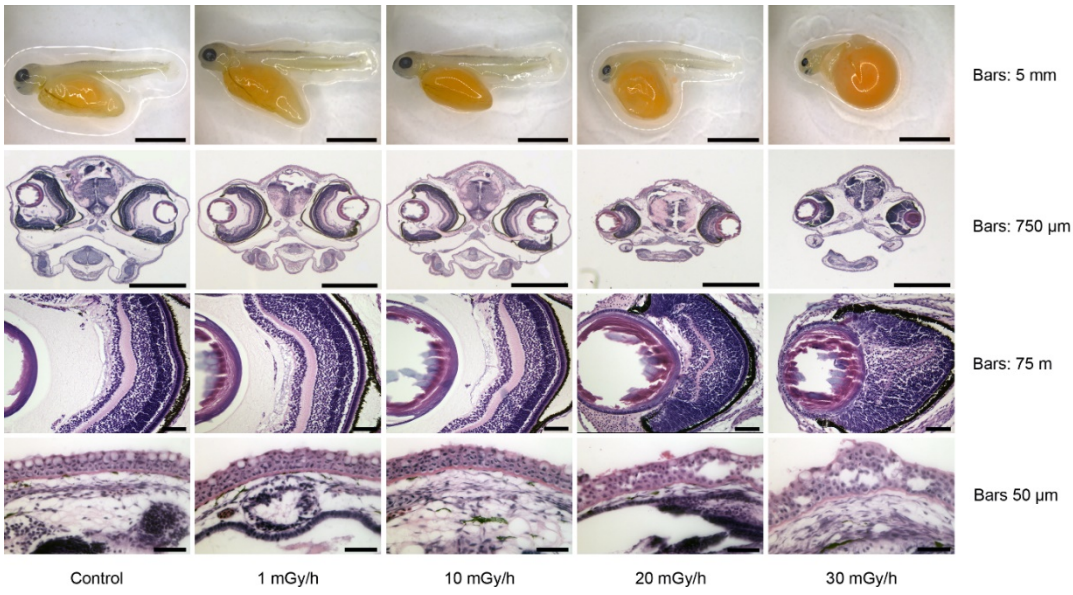

Figure 2.5 Images of salmon embryos exposed to different doses at different dose-rates from fertilization to hatching. The samples are taken immediately after hatching. The first row shows images of salmon alevin immediately after hatching. Second row shows images of transversal sections of the head and eyes, stained with Hematoxylin and eosin. Third row shows enlarged images of the eye, primarily the retina and anterior part of the lens. The fourth row shows enlarged images of the mucus-layer. Adopted from unpublished results by Teien et al.

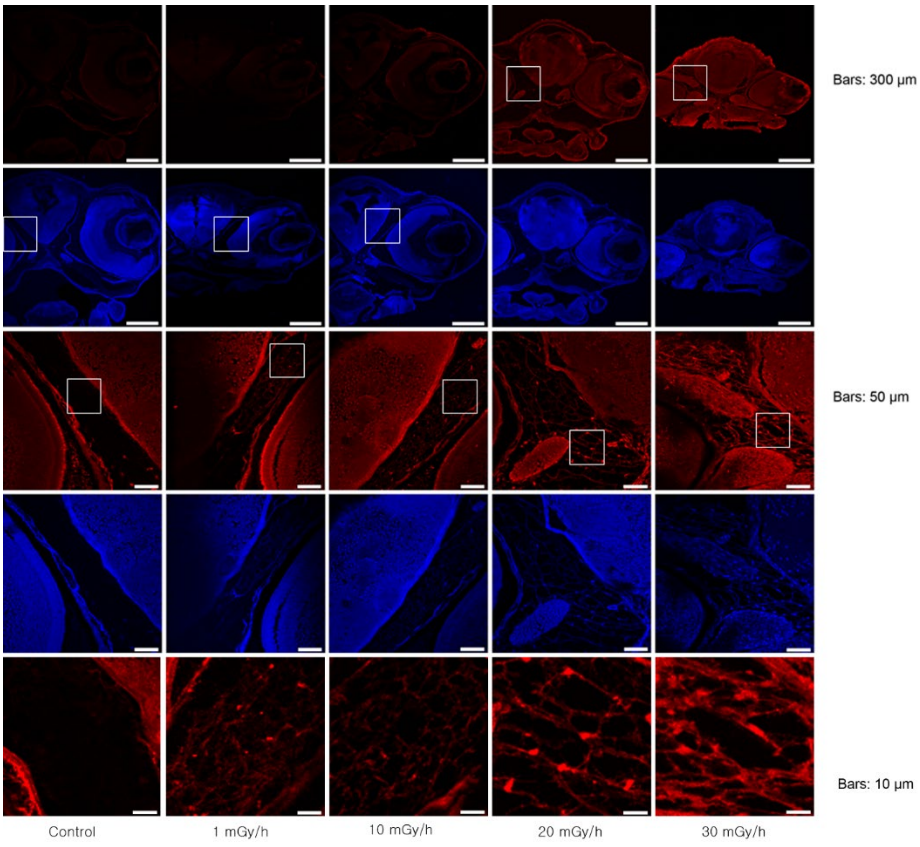

Figure 2.6 Images taken of samples stained with a marker for the apoptotic caspase-enzyme after exposure to ionizing radiationduring the embryonic development. The samples were taken immediately at the end of exposure. The first row shows transversal section of salmon alevin immediately after exposure stained with caspase-antibody. The white square shows the area that is magnified in the third row. The second and fourth row show images stained with Hoechst (nuclear stain). Adopted from unpublished results by Teien et al.

2.5 Fixation of biological samples

Formalin is a cross-linking fixative commonly used for preservation of biological samples that reacts with lipids and proteins, forming covalent bonding with peptides in the protein (Puchtler and Meloan, 1985). Bonding occurs between the uncharged amino-groups of the amino-acids and the oxygen functional group on the aldehyde. The aldehyde-amino acid complex may react further by binding covalently with the amino group of a second protein, forming the cross-link. Cross linkage of proteins preserves tissue well, but causes opacification of the lens, regardless of the presence of cataracts, calling for other means of analysis such as immunohistochemistry.

2.6 Immunohistochemistry

Immunohistochemistry was developed in the early 1940s, and has been a popular technique in medical diagnostics and biological research ever since (Coons et al., 1942). It combines immunology, which is the relationship between antibodies and antigens in biological systems; and histology, which is the study of

tissue and its morphology. The methodology is founded upon the binding properties between antibodies and antigens and utilizes an immunofluorescent marker or a pigmented stain for coloring cells and tissue. Coloring from the stain or fluorescence signal intensity is used as a sign of reaction between antigen and antibody marking the presence of a specific antigen in the tissue.

2.6.1 Binding of antibodies and antigens

Antibodies are a class of proteins that recognize specific antigens and induce a signaling response in cells, stimulating a reaction by the immune system. The distinct Y-shape of the antibodies has a specific function, as the two branches are individual binding-sites that can bind an antigen. The two binding sites at the fork are identical, meaning that they only bind to the same specific antigen. This specificity is what is exploited when performing an immunohistochemical staining.

Immunoglobulin is the most common type of antibody. The heavy chains have a variable and a constant region, linked together in a hinge region (figure 2.7). Two heavy chains are bonded together in the hinge region such that the constant region forms the tail, whilst the variable region forms the fork. A light chain is bonded to each of the variable regions of the heavy chain, together forming the antigen-antibody binding site. The tail of an antibody is referred to as the Fc region, and this part interacts with receptors in the cell surface called Fc-receptors. Different variations in the Fc-region of an antibody gives different properties, as they recruit cells that matches the sequence of the specific region, and therefore dictates the fate of the antibody-antigen complex (Watson et al., 2014).

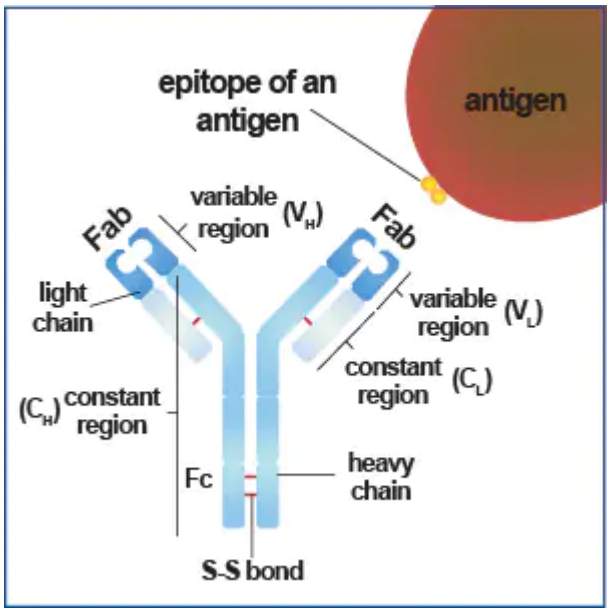

Figure 2.7 An overview of the structure of an antibody. Adapted from NOVUS bio

Antibodies can be either monoclonal or polyclonal. Where the polyclonal immunoglobulins are produced in several different B-cells, the monoclonal antibodies are only produced by a specific line of B-cells. B-cells are lymphocytes, and important parts of the adaptive immune system. Polyclonal antibodies have an advantage over monoclonal antibodies as they have a wider useability due to a higher probability of identifying analogue proteins in different species (Ramos-Vara, 2005), as well as their ability to bind with different epitopes on the same antigen. Monoclonal antibodies will only recognize one specific epitope, giving it a narrower range of application, but offers an advantage of greater experimental reproducibility and the opportunity of comparison between studies. As the antibody only binds to a specific epitope, the certainty that a positive stain is not due to cross linkage etc. makes comparison between staining possible.

2.7 Fluorescence microscopy

When light interacts with matter, either some or all the energy may be absorbed by atoms due to excitation of electrons orbiting the nucleus. Excited electrons absorb the energy carried by a photon with a given wavelength and shifts to an orbital with a higher energy level. The excited electron is highly unstable and quickly de-excite to its original orbital, and excessive energy is emitted as a new photon. It is this absorption-emission principle that forms the basis of fluorescence microscopy (Lichtman and Conchello, 2005). Depending on the distance between the different energy levels, various molecules will absorb and emit light with different wavelengths. Emitted light usually has less energy, and thus a longer wavelength than the incident light. The difference in wavelength between absorbed and emitted light is called the Stokes shift (Sanderson et al., 2014).

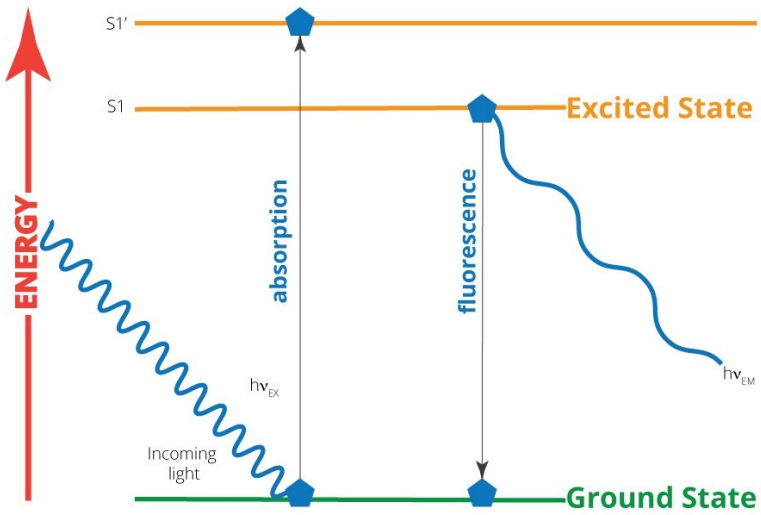

Figure 2.8 Schematic overview of immunofluorescence. Adopted from https://www.wpiinc.com/blog/post/ca-sup-2-sup-detection-in-muscle-tissue-using-fluorescence-spectroscopy

Before the light hits the sample mounted on the microscope it passes an excitation-cube that selects only the wanted wavelengths. Although fluorescent antibodies usually are listed with a maximum peak, they have a broader band of absorption and emission spectra. To prevent overlapping spectra between different fluorescent indicators, the excitation-cube is mounted on the microscope. This excitation-cube is also used to prevent emission light from entering the detector or camera. A dichroic mirror is mounted in the cube at 45° angle from the viewing axis, and the emission light is passed in from the side. Dichroic mirrors reflect incident light that hits the surface at an 45° angle, while light hitting from other angles is transmitted. The emission light is then passed through the sample, and fluorescent light is emitted only nanoseconds later. Emitted light passes through the objective and excitation-cube before it enters the emission-cube containing an emission filter specifically chosen for the wavelength of interest. Another dichroic mirror mounted in the emission-cube then reflects the selected wavelength in the direction of the detector or camera (Sanderson et al., 2014).

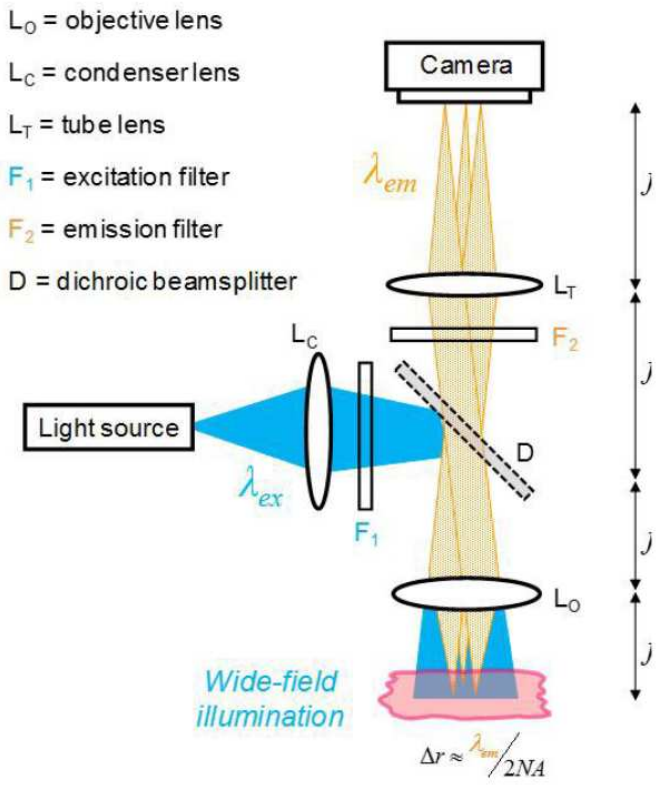

Figure 2.9 Schematic overview of an immunofluorescence microscope. Adopted from https://www.imperial.ac.uk/photonics/research/biophotonics/techniques/fluorescence-imaging-and-metrology/fluorescence-microscopy/

2.7.1 Autofluorescence and photobleaching

Autofluorescence arise when naturally occurring biomolecules with flourophorous abilities are excited and emit light. This phenomenon increases the background signal in fluorescence microscopy. To avoid artifacts of autofluorescence it is necessary to set the exposure level to where background signals are not detected . Although autofluorescence may have different intensities in different parts of the spectral band, the method of lowering the exposure to eliminate background is the best way to ensure as little contribution from autofluorescence as possible.

Photobleaching is another challenge in immunofluorescent microscopy, and happens as the fluorophore in the stain lose its reactivity after prolonged exposure to excitation light and oxygen (Waters, 2013). Samples show less positivity and the image intensity decrease after some period of time due to the bleaching of the fluorescent stain. As this is an inevitable effect from storage or by looking at the samples through the microscope, the only measure of prevention is to reduce the exposure, keep the samples away from the light, and use an anti-fade mounting media that deprive the samples of oxygen. Photobleaching is therefore one of the more limiting factors in the use of fluorescence antigens, and results in a short lifetime of samples stained with such fluorescent antibodies compared to regular hematoxylin-eosin stains.

3. Experimental

3.1 Gamma irradiation of *Salmo salar* embryos

The *S. salar* alevins, or larvae, used in this experiment were exposed to γ-radiation from a Co^{60}-source at the FIGARO facility (Norwegian University of Life Sciences). Eggs from a female *S. Salar* were collected and fertilized before exposure. Fertilized eggs were placed in semi flow-through tanks with 18 liter water reservoir and exposed to nominal doses of 0, 1, 10 and 20 mGy/h from the time of fertilization until hatching (90 days total). Radiation-doses were adjusted by placing the water tanks at different distances from a Co^{60} γ-source at the facility, and the setup is illustrated in figure 3.1. Control of actual received dose was done by placing dosimeters (nanoDot) in the front and back of the tanks, and average doses were calculated based on the two measurements. The eggs were kept in synthetic EPA-very soft water at 6 °C until hatching. All exposures were done according to the OECD guidelines (OECD, 2013).

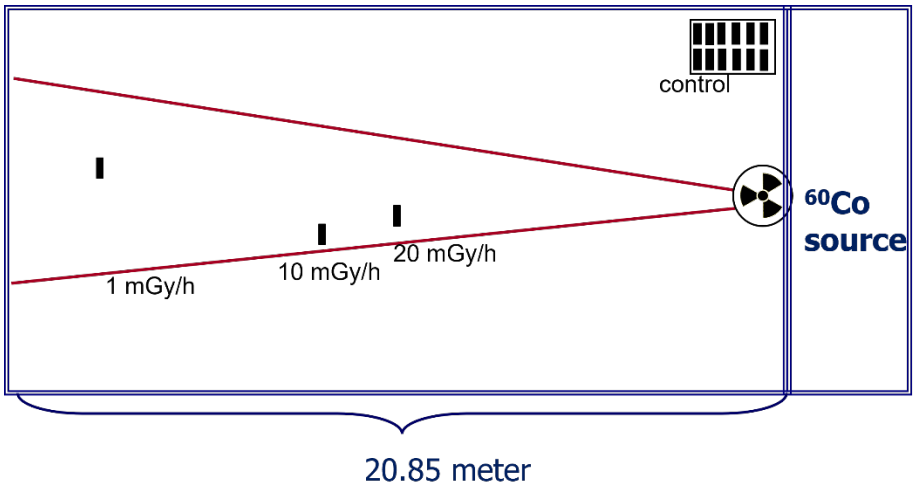

Figure 3.1. Illustration of the exposure setup at the FIGARO facility (Norwegian university of life science, Ås, Norway). Tanks with fertilized fish eggs were placed at different distances from the ^{60}Co source, receiving radiation at dose-rates of 1 mGy/h, 10 mGy/h and 20 mGy/h. The control group is placed in the shade of the γ-radiation beam (top right corner).

After hatching, some alevins were sampled immediately for analysis of acute exposure (results are presented in chapter 2.4.1, figure 2.5 and 2.6), while the remaining specimens were moved to the fish laboratory facility (Norwegian university of life science, Ås, Norway) for recovery. The alevins were recovering for three months at 9°C with the same water-quality as during exposure and transitioned to the fry stage during this period. The water reservoirs were increased to 100 liters during recovery, and the reservoir-tanks were continuously aerated by bubbling, and a CO_2-stripper was mounted to prevent accumulation of CO_2 over time. The recovering alevins were given no feed, as they still fed on their yolk sac during most of the recovery-period. An image of the fry (alevin after recovery) at the time of sampling is presented in figure 3.2.

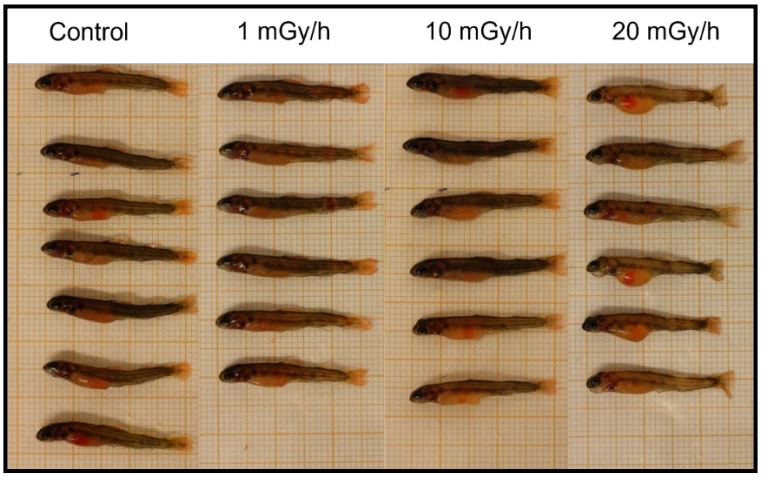

Figure 3.2. Salmon fry (Salmo salar) 90 days after exposure. The images are taken at the time of sampling.

3.2 Preparation of formalin and fixation

Formalin was prepared from para-formalin powder in batches and then stored in a freezer. Sixteen grams of paraformaldehyde was dissolved in 300 ml dH_2O, and 2 ml of 1M NaOH was added and dissolved at 60 ℃ using a magnetic stirrer. After dissolving the powder, the solution was cooled to room temperature before adding 40 mL of 10x phosphate buffered saline (PBS). The PBS was prepared by dissolving 2 tablets (SIGMA) in 60 mL of dH_2O. After addition of PBS, the pH was adjusted to approximately 7.4 by adding concentrated HCl dropwise. Total volume was then adjusted to 400 mL with the remaining PBS, and 50 mL was aliquoted to 100mL containers for storage in the freezer. The chemical is unstable in highly concentrated solutions and the molecules polymerize quickly if the solution is kept at room temperature. This reduces reactivity and lifetime of the fixative, and the chemical is usually kept as a powder in the form of paraformaldehyde for long term storage at room temperature (Puchtler and Meloan, 1985). Before use, the solution was thawed and diluted to 2% concentration by adding 50 mL dH_2O to the 100 mL container.

After euthanization, the salmon fry (alevin after recovery) were fixed with 2.5 ml fixative for 0.5 mL sample in a solution of 2% formalin, and stored at 4 ℃ from March 2016 to March 2021. The samples were kept in formalin for the whole period.

3.3 Tissue processing

To allow sections of soft tissues, embedding in a supportive media, alternatively cryopreservation, is needed. Before sectioning, whole *S. salar* fry were dehydrated and infiltrated with paraffin. First, *Salmo salar* fry were dehydrated manually by submersion in a gradually increasing concentration of EtOH prepared in 50 mL falcon tubes from concentrated alcohol (100 %) diluted with dH_2O to concentrations of 30 %, 50 % and 70 %. All samples from the same group were displaced from the formalin, and residual fixative was rinsed using 30 % EtOH. Samples from the same group were then placed in 50 mL falcon tubes with fresh 30 % EtOH for 1 hour at room temperature, then transferred to 50 % EtOH falcon tubes for 2 hours at room temperature, before overnight incubation in the refrigerator. Lastly, the samples were incubated in new 50 mL falcon tubes with 70 % EtOH for 2 hours at room temperature. After incubation at room temp, all samples were transferred to falcon tubes with fresh 70 % EtOH and stored in the freezer until further use.

The remaining dehydration and infiltration steps were automated using a Tissue-Tek® VIP™ 5 Jr (Sakura Finetek, USA). Each sample was placed in an individual cassette marked with a pencil before placement in the Tissue-Tek®. Using a pencil is important as other markers may be washed away with

alcohol or xylene. The Tissue-Tek® program used changes of 70 %, 80 % and 90 % EtOH (35 ℃) for 15 min each before washing with 3 changes of 100 % EtOH (35 ℃), lasting 30 minutes, 30 minutes and 1 hour respectively. A summary of the program is given in table B.1.

Alcohol is an aqueous solution and therefore not miscible with paraffin. Xylene can be mixed with both EtOH and paraffin and was used as a clearing agent. This step consisted of three 30-minute changes of xylene at 35 ℃, 45 ℃ and 50 ℃, respectively, before infiltration with four changes of paraffin at 58 ℃. Each change of paraffin lasted for 1 hour. The samples were prepared in the afternoon and the infiltration process was performed overnight, leaving the samples in the last change of paraffin until embedding the next morning.

Before embedding, after dehydration and infiltration, all samples were dissected. The heads were removed from the rest of the body with a scalpell, and embedded separately in paraffin using a Tissue-Tek® TEC™ 5 (Sakura Finetek, USA). Only the heads were used further in this experiment, and they were embedded ventral side down to allow sectioning of the frontal plane. The alevin bodies were also embedded for storage purposes.

To investigate the impact of different tissue processing and fixation procedures on sectioning, eyes from Atlantic salmon parr were dissected after suggested protocol (Wildgoose, 2007). The periocular skin attaching the eye to the orbital rim was carefully cut with a small scalpel, making sure not to damage the eye globe. The eye was carefully lifted out of the socket (enucleation) with a dull spatula as far as possible without damaging it. A pair of sharp curved scissors were used to cut the optic nerve located in the ventral region, leaving as much as possible attached to the eye. Three fish were euthanized, and a total of 6 eyes between 10-15 mm in diameter were sampled. The eyes were fixed in 2 % and 4 % formalin for 24 and 48 hours, injecting some of the fixative using a small syringe.

After fixation, the eyes were dehydrated and placed in 70% EtOH following the same steps as done with the salmon fry. Before the remaining dehydration steps, all eyes were dissected. Sagittal cuts were made with double edge razorblades, removing as much of the scalp as possible without disturbing the lens or lens-suspension found in the dorsal-ventral plane of the eye. After dissection, the samples were placed in cassettes and stored in a Thermo Scientific ™ Excelsior™ AS tissue processor with formalin while awaiting to be processed. The dissected eyes were then dehydrated following the default program used by the pathology department at the faculty of veterinary medicine (NMBU). After processing, the infiltrated samples were embedded in paraffin blocks for sectioning.

3.4 Sectioning and staining

3.4.1 Sectioning

Frontal sections at 3.5 µm thickness were made using a Leica microtome and mounted on microscope slides. Trimming of the paraffin blocks was done at 20 µm thickness until the lens was visible, and the plane was then leveled to ensure symmetry. To improve section quality, the paraffin blocks were placed tissue side down on a block of ice, slightly rehydrating the brittle tissue of the crystalline lens and to cool down the paraffin. The blocks were remounted on the microtome and sectioned. Three sections were mounted on each microscope slide, giving 20 slides in total, dried for 1 hour at 38 ℃ and finally at 60℃ over-night. Total number of replicates was n=14 for each antibody, where the group sizes were n=4 for the control, 1 mGy/h, and 10 mGy/h, and n=2 for the 20 mGy/h dose-rate.

For deparaffinization, 5 slides were placed in slide-carriers and washed in two 5 minutes changes of xylene before rehydration in absolute EtOH. Sections were then rinsed briefly in two changes of 96% EtOH, and then one change of 70 % EtOH, one change of distilled water and finally tap water to complete the rehydration steps. All steps were done under a fume hood, and the slide-carriers were fully submerged in every bath. The slide-carriers were tapped dry on tissue paper in between rinsing-solutions.

Fixation with formalin may form cross-linkage between proteins in the tissue, masking the epitopes of the antigen. By heating the samples in a solution of hydrogen peroxide, the cross-linked bonds are broken, and some of the reactivity may be retrieved. This process is called antigen-retrieval, and its necessity varies depending on which antibodies are to be used. This step was omitted in the current experiment.

3.4.2 Hematoxylin and eosin (HE) staining

Histology was assessed by hematoxylin and eosin staining. After rehydration, the samples were placed in a hematoxylin bath for 10 minutes. The sample rack was then placed in a container and rinsed with running tap-water for 10 minutes, making sure the samples were not hit directly by the stream. The slides were then placed in a container with eosin staining for 10 minutes. After staining with eosin, the samples were dipped quickly in a container with tap water, and rinsed briefly (a couple of seconds) in increasing concentrations of EtOH (dH_2O, 70 % EtOH, 90 % EtOH and absolute EtOH). The samples were then soaked in xylene for 2x 1 minute before application of mounting media. The samples were still wet with xylene upon application of mounting media and coverslip. All steps involving EtOH and xylene were performed under a fume hood.

3.4.3 Immunofluorescent labeling

For immunofluorescent labeling, slides were placed tissue side up in a humidity-tray in batches of 10 after rehydration and kept there for the remainder of the staining procedure. This was done to prevent drying of the tissue, as it could introduce artifacts. Permeabilization of the tissue was done by incubating the samples with Triton-X for 10 minutes, making sure the entire sample was covered. Permeabilization is required to ensure successful penetration of the different membranes after fixation with formaldehyde-based fixatives. The permeabilization detergent dissolves the lipid membranes of the cells and makes intracellular antigens more accessible for the large antibodies, thus enhancing binding and signal strength. Triton-X was washed with 1x Dulbecco's Phosphate Buffered Saline (DPBS) (Gibco™) for 3 changes of 3 minutes each, covering the entire slide with solution.

After washing, a hydrophobic barrier was drawn around each sample with a PAP pen to prevent cross contamination and reduce the amount of antibody-solution needed to fully cover the tissue. The samples were blocked for 60 minutes with 70 µL of 5% serum to prevent nonspecific binding between antibodies and the tissue. The blocking solution was removed with tissue paper, and the samples were washed with DPBS for 3 minutes by covering the samples inside the hydrophobic circles (approximately 70 µL).

The selection of antibodies used in the analysis was based on expected effects from radiation found in the literature. Due to the high specificity to certain species, a screening of several antibodies was performed on a series of samples. Only the antibodies showing positive labeling was selected for further analysis. Different colored secondary antibodies were also tested, and the rhodamine secondary antibody was selected as it yielded the best results during imaging. After selection of antibodies, the procedure was repeated on three more replicates from each dose giving 4 replicates from each group. Only one replicate from the 20mGy/h group was available for the second round of staining, as the sample size was lower from this exposure. The primary antibodies used for screening are listed in table 3.1. Antibodies were prepared and diluted according to the manufacturer's recommendations.

For detection of the nuclear protein Ki-67, proliferative cells and cell death, Ki-67 rabbit monoclonal antibody (Thermo Fisher Scientific, UK), Anti-Proliferating Cell Nuclear Antigen (PCNA) monoclonal mouse antibody (DakoCytomation, Denmark), and Caspase-3 rabbit monoclonal antibody (Cell Signaling Technology®, Massachusetts, USA) were used respectively.

For investigation of the BER repair mechanism, 8OHdG mouse monoclonal antibody (Santa Cruz Biotechnology, INC., Texas, USA), 8-oxoguanine-DNA glycosylase (OGG1) polyclonal rabbit antibody (NOVUS Biologicals®), Apurinic/apyrimidinic endonuclease 1 (APE1) monoclonal mouse antibody

(Enzo Life sciences INC.), and anti-DNA polymerase-β polyclonal rabbit antibody (ABCAM) were used for detection of 8-hydroxy-2'-deoxyguanosine, glycosylase expression, apurinic/apyrimidinic endonuclease expression, and polymerase activity respectively.

For detection of fibrotic tissue and autophagy, anti-α smooth muscle Actin monoclonal mouse antigen (ABCAM) and Microtubule-associated protein 1 light-chain 3 (LC3) polyclonal rabbit antigen (NOVUS Biologicals ®) were used respectively. Dilutions was done with 0,5 % bovine serum (SIGMA) at a ratio of 1:100 for APE1, OGG1 and 8OHdG; 1:150 for Pol-β, and 1:200 for αSMA and LC3. The antibodies were kept on ice until application. Total volume was 800 µL for each antibody,

Table 3.1 Overview of antibodies used in this experiment, their dilution ratio and manufacturer. The species from which the antibodies are extracted is listed in the species column. The different molecular endpoints they are labeling are listed in the Endpoint column.

Antibody	**Species**	**Clonality**	**Dilution**	**Endpoint**	**Manufacturer**
Ki-67	Rabbit	Mono	1:200	Proliferation	Thermo Fisher Scientific, UK
PCNA	Mouse	Mono	1:1500	Proliferation	DakoCytomation, Denmark
Caspase-3	Rabbit	Mono	1:200	Apoptosis	Cell Signaling Technology® ,Massachusetts USA
8OHdG	Mouse	Mono	1:100	Oxidative damage	Santa Cruz Biotechnology, INC. Texas USA
OGG1	Rabbit	Poly	1:100	BER enzyme	Novus Biologicals®
APE1	Mouse	Mono	1:100	BER enzyme	Enzo Life Sciences INC.
DNA pol-beta	Rabbit	Poly	1:150	BER enzyme	ABCAM
Alpha-SMA	Mouse	Mono	1:200	Fibrosis	ABCAM
LC3	Rabbit	Poly	1:200	Autophagy	Novus Biologicals®

All samples were then incubated at room temperature for 1 hour with the lid of the humidity chamber closed to prevent the samples from drying out, and then incubated at 4°C overnight. The primary antibodies were removed using a tissue paper to prevent cross contamination, and the samples were washed 3x 10 minutes with 1x DPBS. Fluorescent secondary antibodies are light sensitive, and all the remaining steps were therefore carried out in darkness. Removal of antibodies was done swiftly, and the samples were never allowed to dry out as this would temporarily increase antibody concentration and could possibly introduce artifacts. All staining steps were therefore, as mentioned, performed in batches of 10 slides.

The secondary antibodies were diluted according to manufacturer's recommendations, with a concentration of 1 part antibody to 1000 parts diluent. After washing, approximately 70 µL of secondary antibodies were applied with a micro-pipette to each sample. The samples were then incubated at room temperature for 1 hour before washing in three 5 minutes changes of 1xDPBS. Nuclear staining was done

with Hoechst nuclear stain diluted 1:1000 in 1xDPBS, and the samples were incubated for 15 minutes at room temperature after application. Excess nuclear staining was washed away in 3 changes of 1xDPBS prior to application of an anti-fade mounting media and coverslip. All sections were then left to dry and harden in the refrigerator overnight before imaging.

Negative controls were prepared to ensure that non-specific binding between the secondary antibody and the samples did not affect the results. The negative controls followed the same procedure as the normal samples, but instead of a primary antibody they were incubated with DPBS.

3.5 Fluorescence microscopy

All images were taken on a Zeiss Axio Imager M.1 fluorescence microscope with a Zeiss AxioCamMR3 camera at 4x, 10x and 40x magnification. For the fluorescent images, red channel (Rhodamine) was used for antibody detection, green channel was used to adjust exposure and minimize background signals caused by autfluorescence, and the blue channel was used for the Hoechst nuclear counter-staining. The exposure was set manually, aiming at reducing the background signal without compromising the signal intensity. The same exposure settings were used for all images of the same sample at the same magnification level for comparison purposes. Exposure of different samples were adjusted individually as slight variations in background between the samples were expected. All images were captured in the AxioVision Software, and the nuclear stain images were merged with the red channel images within the software. Brightfield images were also taken for each sample to serve as a reference point for recognition of potential artefacts, tissues and regions etc.

3.6 Interpretation of images

To quantify the positivity of the stains and evaluate the results from the staining, all images were evaluated individually by three different people, two of which were experts from the Center of eye research at the Oslo University Hospital. All images were interpreted semi-quantitatively by scoring from 0 to 3 with intervals of 0.5. Negative samples were given score 0, low signal was 0.5 etc. and 3 was strong signal. However, due to the small number of comparable samples from each group, no statistical analysis was performed on the data, the final evaluations were done qualitatively.

4. Results

4.1 Method optimization

Histological changes and molecular responses in *S. salar* fry exposed to γ-radiation during development were assessed by hematoxylin and eosin (HE) staining and immunofluorescent labeling respectively. Images of eyes sampled from non-irradiated salmon parr (HE-stained) are provided in figure 4.1 and were used to assess the method and impact of fixation procedure on sectioning and staining properties. The protocol for fixation and tissue preparation of eyes from larger salmon (parr) yielded sections where the cornea, lens and retina were intact (figure 4.1). Tissue-structure was preserved to a level where the different regions of the eye were easily recognizable and cell nuclei could be distinguished from the cytoplasm. The different stages of differentiation in LECs could be seen in the posterior region of the lens (image D in figure 4.1). In HE stained samples, nuclei were colored dark blue-purple, while cytoplasm could be seen as pink.

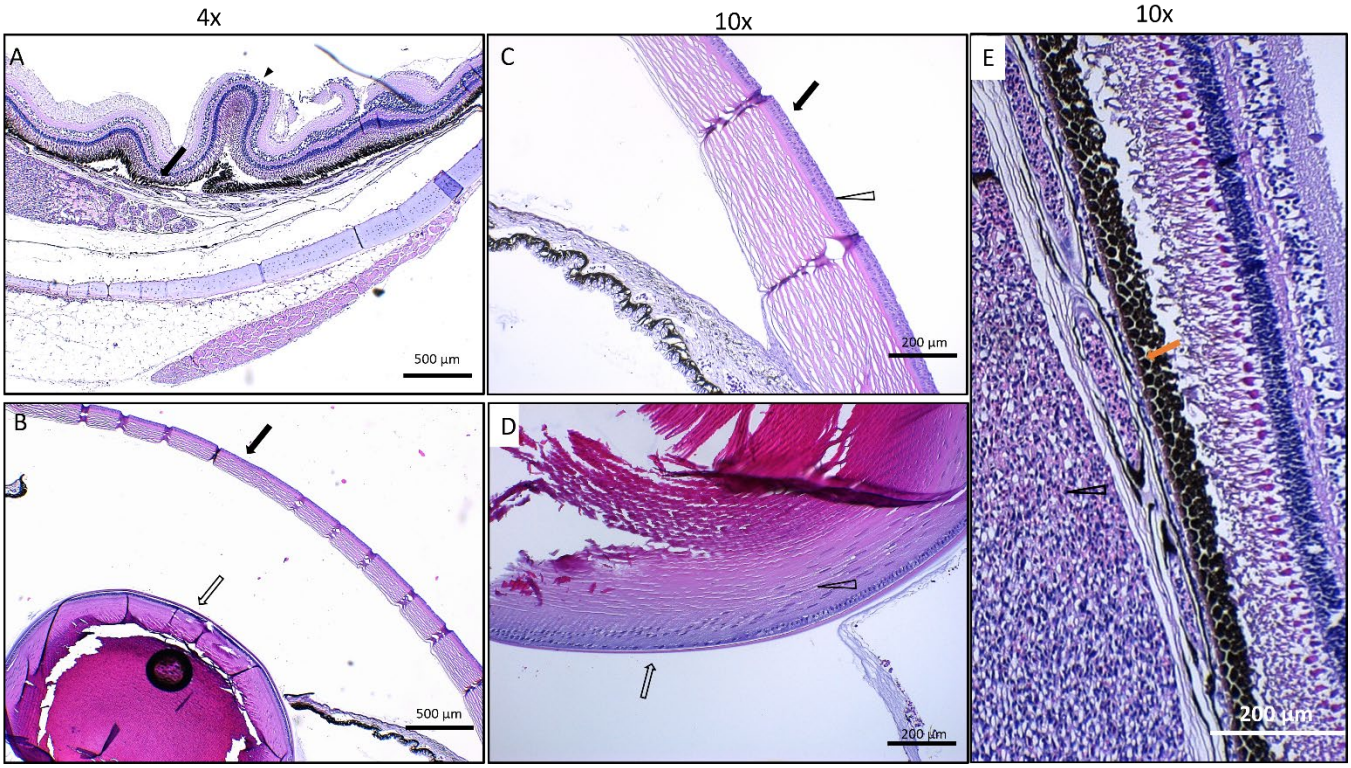

Figure 4.1 Sections from salmon eyes stained with Hematoxylin and Eosin. A) 4x magnification of the retina. Some tissue artifacts could be seen because of sectioning (arrowhead). Retinal pigment epithelium (RPE) was also visible (arrow). B) 4x magnification image of cornea (black arrow) and lens (hollow arrow). C)10x magnification image of the cornea (arrow) from the limbal region. Cell nuclei were visible as purple ovals (white arrowhead). D) 10x magnification of the posterior lens-region. Differentiating cells that have not yet lost their nuclei were visible (arrowhead). These had an elongated shape, compared to the less differentiated epithelial cells (arrow). E) 10x magnification image of the retina. RPE cells were visible (orange arrow).

Sections of exposed *Salmo salar* fry are presented in figure 4.2. The images showed intact tissues with no apparent artifacts or influence from preservation procedure, both in the ones manually dehydrated and dehydrated using the automated Tissue-Tek VIP. Quality of sections were assessed by investigating the conservation of tissue, including the brittle lens, and immunoreactivity. However, some tissue shrinkage due to fixation could be observed as bends in the retina. A noticeable decline in section-quality with increasing time after mounting on the microtome was seen, illustrating the importance of keeping the blocks cooled before sectioning (results not presented).

Despite prolonged storage in formalin, sections from *S. salar* fry yielded positive images after labeling with fluorescent markers (figures 4.6 to 4.16). The same accounts for sections stained with HE. No effect such as decreased reactivity could be seen by comparison of images from figures 4.1 and 4.2, although the samples presented in figure 4.2 were stored on formalin for several years longer than the ones presented in figure 4.1.

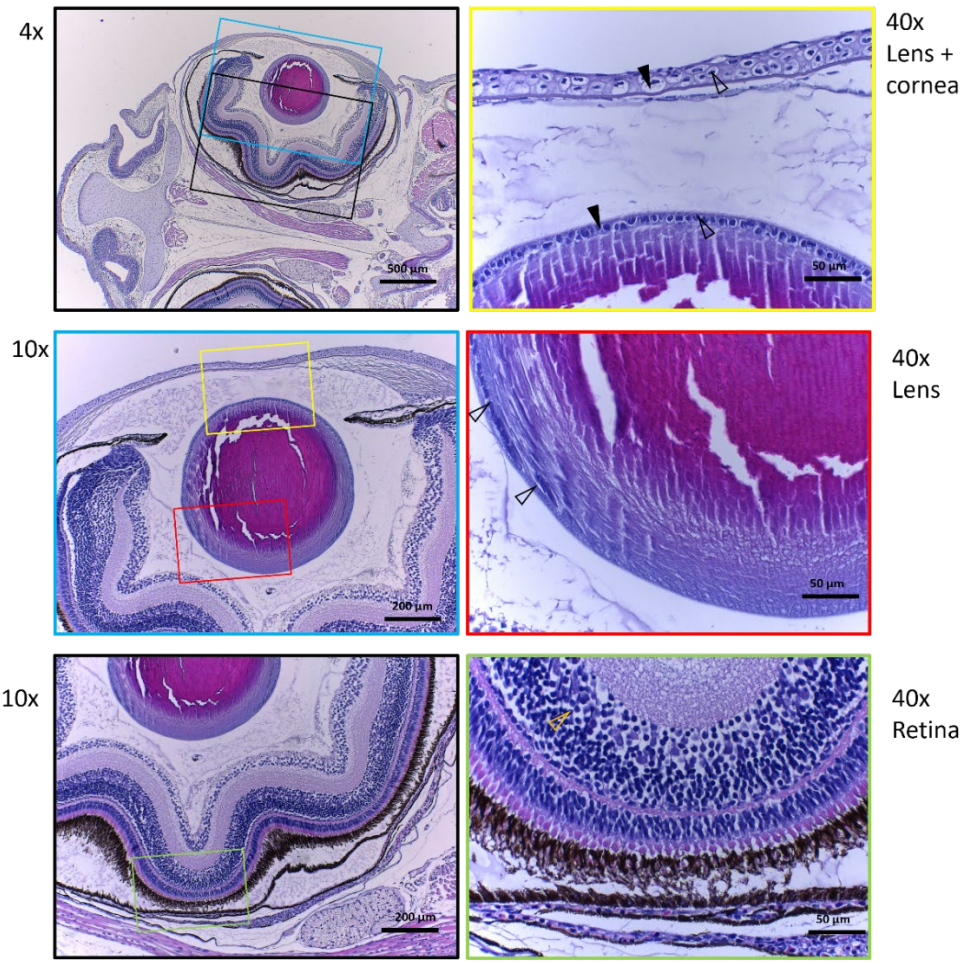

Figure 4.2 Hematoxylin and Eosin staining of Salmo salar *exposed to 10 mGy/h of radiation during embryonic development. The cellular structures were well conserved, and the nuclei of cells were easily distinguishable due to the purple staining (hollow arrowhead). Some cracks in the lens were visible, but most of the fiber cells appeared intact. The cytoplasm (arrowhead) was visible as empty areas surrounding the nuclei, and pink areas in the lens and retina.*

4.2 Long term histological and morphological changes in the ocular tissues

At 90 days post irradiation, no histological differences were observed between the groups, indicating high extent of recovery from any previous tissue effects. All samples showed similar development of cornea, lens and retina although slight variations in the diameter of the lens could be seen between samples. No difference in organization of LECs in the epithelial layer could be attributed to the dose-rate (figure 4.3). The lack of HE stained images from the 20 mGy/h group was compensated by using Hoechst nuclear stained images (figure 4.4). Images of Hoechst were only used to assess the organization, size and distribution of cell nuclei, in addition to the distribution of layers in the retina. The images were not used to assess any damage or lesions in the different tissues.

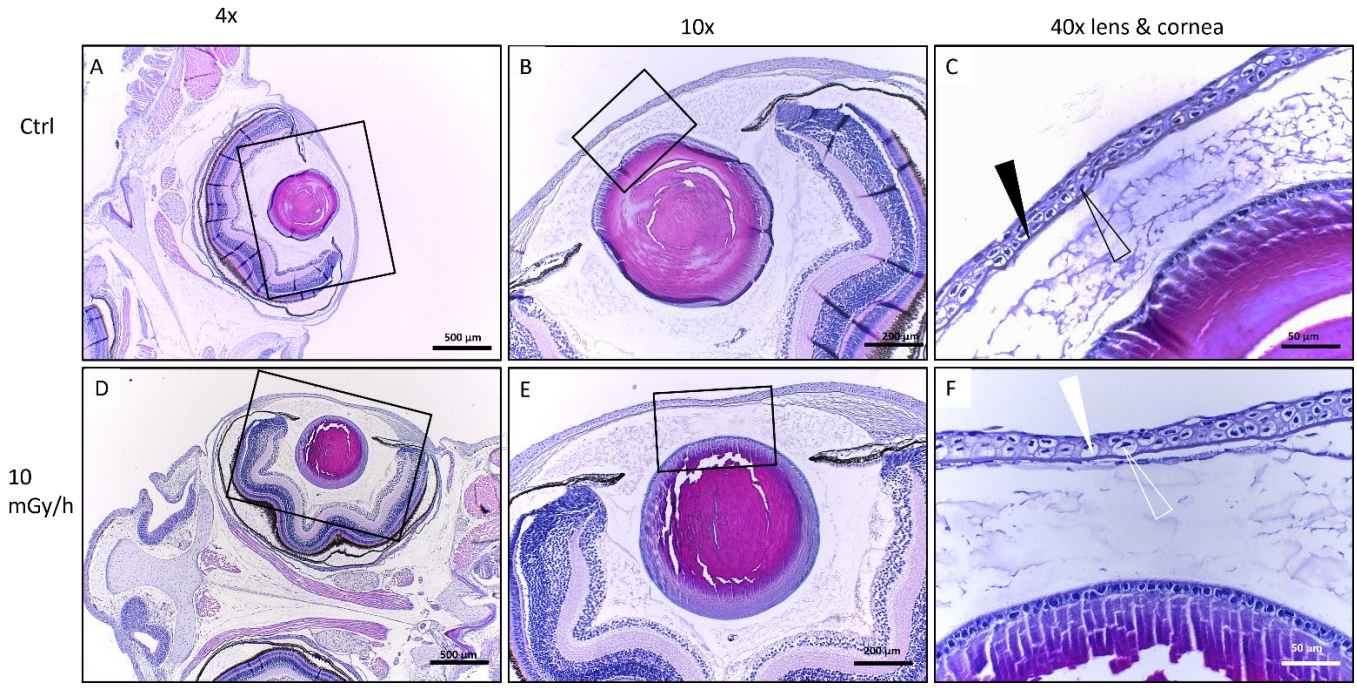

Figure 4.3 Representative selection of HE stained samples. A) Overview of fish from control group. B) 10x magnification of the cornea and lens from control group. C) 40x magnification of cornea and lens from control group. D) Overview of fish receiving γ-radiation at 10 mGy/h during embryonic development. E) 10x magnification of cornea and lens from fish receiving γ-radiation at 10 mGy/h during embryonic development. F) 40x magnification of cornea and lens from fish receiving γ-radiation at 10 mGy/h during embryonic development. Cell nuclei (hollow arrowhead) and cytoplasm (arrowhead) were clearly visible in the cornea and lens.

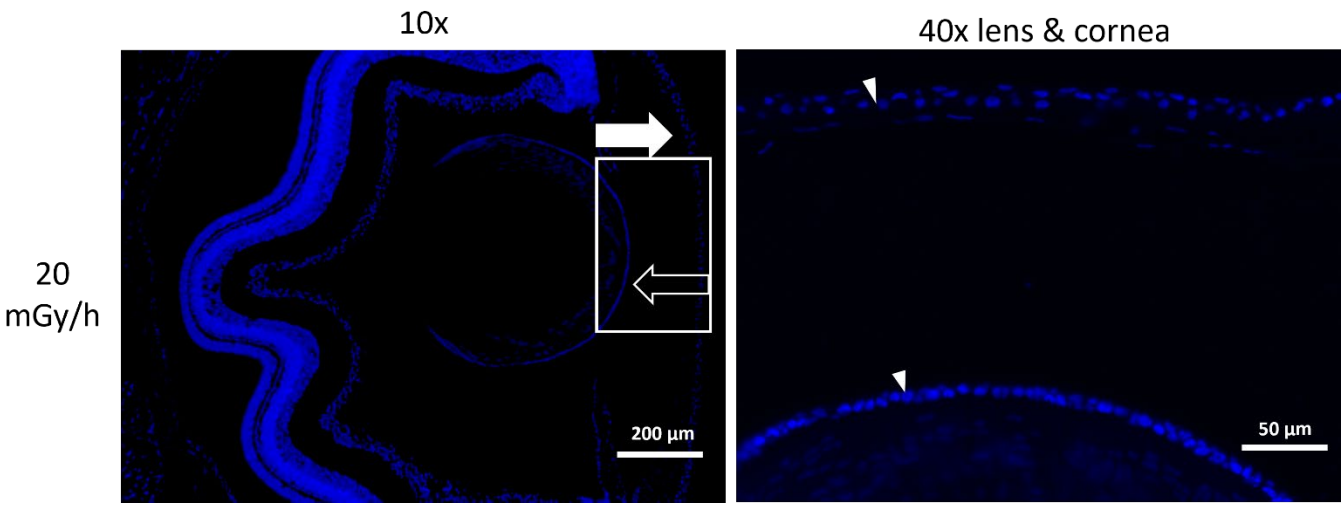

Figure 4.4 Immunofluorescent images of Hoechst nuclear stained samples receiving 20 mGy/h of radiation. The nuclei can be seen as blue ovals (arrowhead) both in the cornea (white arrow) and lens (black arrow)

No histological differences in the retina could be observed between individuals from the control group and 10 mGy/h dose-rate (figure 4.5). The retinal layers appeared organized and were easily distinguishable from each other. Also, the difference in development seen in samples analyzed immediately after exposure (figure 2.4 and 2.5) was no longer visible after recovery. The lens and retina were clearly separated in the individual exposed to 20 mGy/h after recovery, and the retinal layers were pronounced and recognizable (figure 4.4), resembling the development of the other samples.

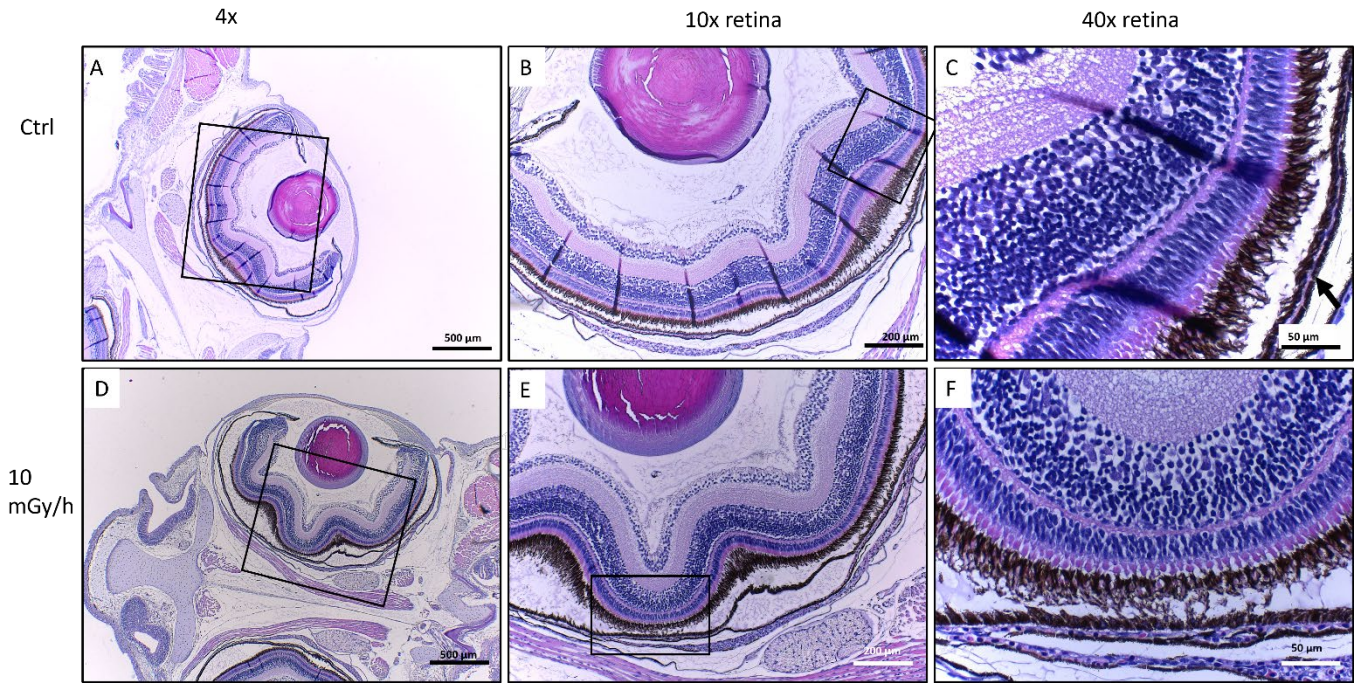

Figure 4.5 Representative selection of HE stained samples. A) Overview of fish from control group. B) 10x magnification of the retina from control group. C) 40x magnification of retina from control group. D) Overview of fish exposed to γ-radiation at 10 mGy/h during embryonic development. E) 10x magnification of retina from fish exposed to γ-radiation at 10 mGy/h during embryonic development. F) 40x magnification of retina from fish exposed to γ-radiation at 10 mGy/h during embryonic development. Nuclei (hollow arrowhead) and cytoplasm (arrowhead) were clearly visible in the cornea and lens.

4.3 Expression of apoptotic and proliferative markers

Neither the apoptotic (caspase 3) or proliferative (PCNA or Ki67) markers were detected in any sample. The antibodies used were not native to fish or previously tested for compatibility with *Salmo salar*. Images of the Hoechst nuclear stain confirmed the samples integrity, thus the lack of signal in the rhodamine channel (red) was attributed to the lack of binding between antibody and antigen. As no positive control was available, it is not known whether the absence of signal is due to incompatibility between antibodies and the *Salmo Salar* species, or if the samples were truly negative for the markers used.

4.4 Microtubule associated protein light-chain 3 (LC3)

Autophagy was investigated by labeling with the LC3 antibody, but only low levels of detection were found at all dose-rates. To determine the localization of antigens within the different tissues and cells, the brightness and contrast were enhanced during post-processing of the images. The same was also done with images from the green channel to avoid false positive signals due to autofluorescence (Figure A.1.).

LC3 was detected mainly in the epithelial layer of the cornea (figure 4.6). In image A.2 of figure 4.6, the cornea was twisted, resulting in an artefactually increased signal intensity from this region due to a

thicker layer of cells, not due to actual autophagy. A weak signal could be seen in the epithelial layer of the lens (white arrowhead in image B2 of figure 4.6), and some positive labeling was detected in the OFZ (dotted arrow) in image A.1 and B.1. Signals from the retina were weak, with more autofluorescence compared to the other tissues (figure A.1). No observable dose-response relationship between radiation and autophagy was found in any of the tissues after three months of recovery from exposure to ionizing radiation.

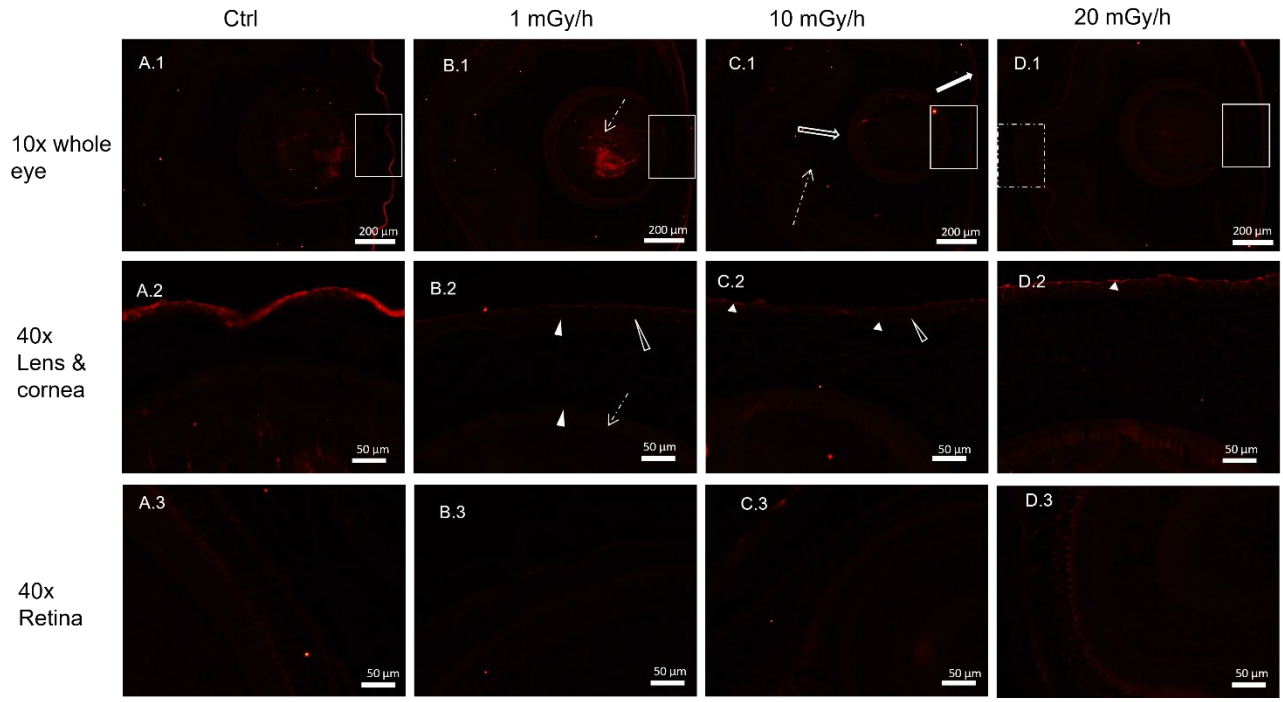

Figure 4.6 Representative immunofluorescent images of LC3 labeled samples. A) Control group. B) Individual exposed to γ-radiation at 1 mGy/h during embryonic development. C) Individual exposed to γ-radiation at 10 mGy/h during embryonic development. D) Individual exposed to γ-radiation at 20 mGy/h during embryonic development. Brightness and contrast were increased in software for illustration purposes. Some detection was seen in the corneal epithelium (white arrowhead in image C2 and D2), and in the organelle free zone (OFZ) (dotted arrow image B1).

4.5 Alpha-Smooth-Muscle Actin (α-SMA)

Radiation induced fibrosis was assessed by labeling with alpha smooth-muscle actin (α-SMA). Expression of α-SMA was found in samples from all groups after recovery. In the cornea, the signal was strongest in the epithelial and endothelial borders with some cytoplasmic localization in cells from the stroma, although determining the exact cellular localization was difficult at the magnification-levels used. In the lens, expression was most prominent in the LECs, but some residues were also found in the lens fiber cells outside the OFZ. There was a strong signal in the epithelial layer (image B.1, figure 4.7), but this was regarded as artifactual as tissue was twisted. Figure 4.8 present an enlarged version of image C.2 from figure 4.7 and illustrates the cellular localization of the signal in the cornea and lens. In the retina,

detection was seen in the non-laminated region, decreasing gradually towards the central part of the retina.

Despite detectable levels of the enzyme, no fibrosis or mesenchymal cells were seen in samples stained with HE (Figure 4.3). A slight increase in detection was seen in the 10 and 20 mGy/h groups compared to the control and 1 mGy/h group. This was most obvious in the lens fiber cells found outside the OFZ (dotted arrow image C.1 in figure 4.7).

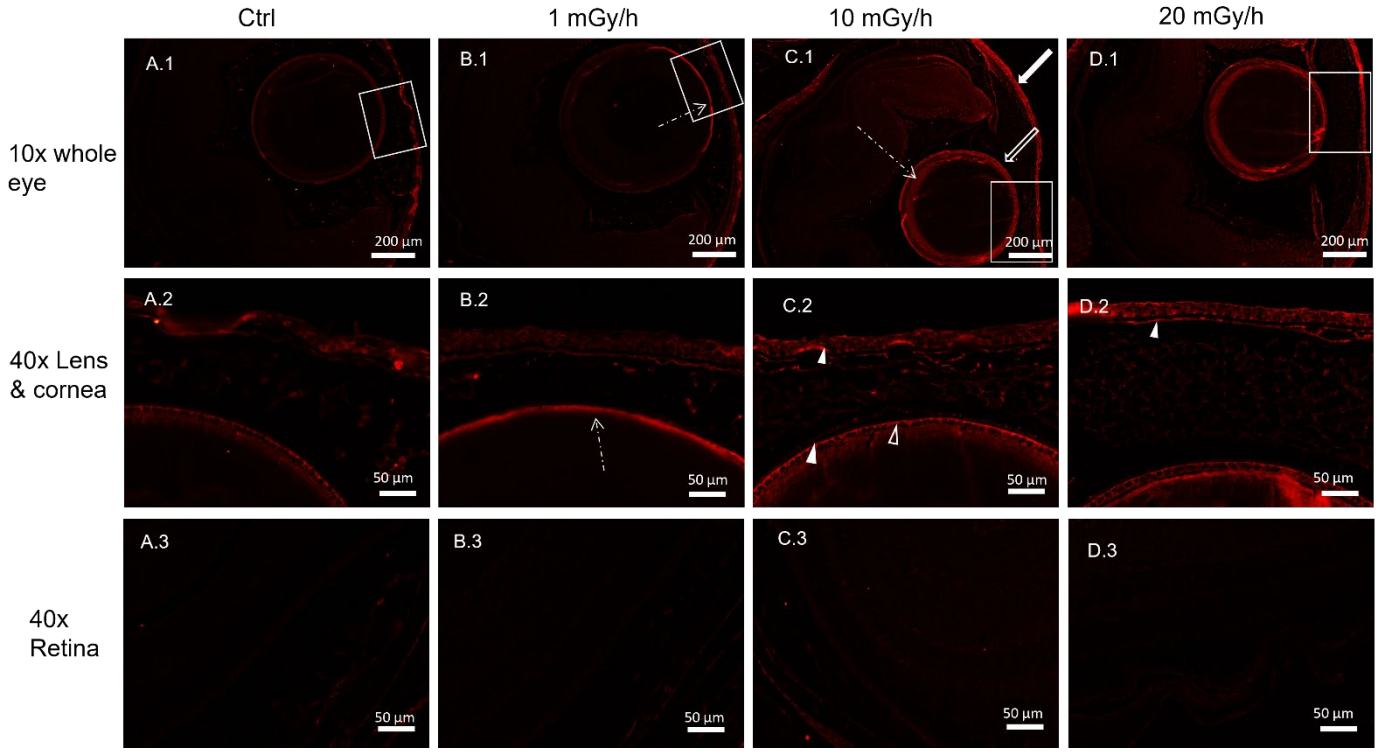

Figure 4.7 Representative selection of immunofluorescent images of SMA-α stained samples. A) Control group B) Individual exposed to γ-radiation at 1 mGy/h during embryonic development. C) Individual exposed to γ-radiation at 10 mGy/h during embryonic development. D) Individual exposed to γ-radiation at 20 mGy/h during embryonic development. Expression was seen in cornea (white arrow) and lens (black arrow). Expression was seen in the cytoplasm (white arrowheads), but no expression was found in the nuclei (black arrowhead). An artifact due to folding of the lens epithelial layer in image B.1 and B.2 was seen (dotted arrow).

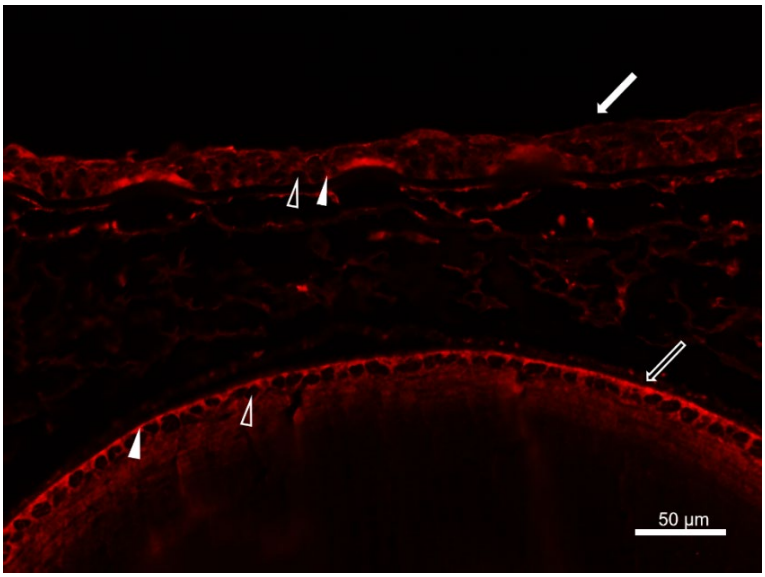

Figure 4.8 Immunofluorescent image showing α – SMA labeled cells in the cornea (white arrow) and lens(black arrow) from fish exposed to 10 mGy/h of γ-radiation during embryonic development. The signal was most prominent in the cell cytoplasm (white arrowhead), and the nuclei were visible as black dots (black arrowhead).

4.6 Localization of cytoplasmic 8-hydroxy,2-deguanosine (8OHdG)

Labeling the samples with 8-hydroxy,2-deoxyguanosine showed that the oxidized guanosine base was present in all samples after the recovery period (figure 4.9). Signals were detected in the cornea, and the images taken at 40x magnification showed that oxidized guanosine bases were localized predominantly in the cell cytoplasm (figure 4.10). The cell-nucleus could be seen as dark ellipses, indicating little or no detection of antibodies, suggesting little oxidative damage to the nuclear DNA. Oxidized bases were detected in the lens, both in the epithelial layer and outside the OFZ. Similar to the cornea, the signal was primarily localized in the cytoplasm (figure 4.10). Low levels were detected in the nuclei as well, though considerably less than what was found in the cytoplasm. Detection in LECs was most prominent in the anterior part of the epithelial monolayer, as seen in the 10x magnification images. Oxidized guanosine bases were mostly located in the cell-cytoplasm in all samples, implying a higher degree of oxidative damage to mRNA and mtDNA. Almost no signal was found in the retina, indicating little oxidative damage to DNA or mRNA in this tissue.

Detection of 8OHdG in the control group also suggested a high presence of oxidatively damaged DNA or mRNA in *S. salar* fry developed from unexposed eggs. No dose-dependent relationship between dose-rate and presence of oxidized guanosine bases was found after a period of recovery from exposure to γ-radiation. Negative controls were used to uncover any unspecific binding of the fluorescent marker.

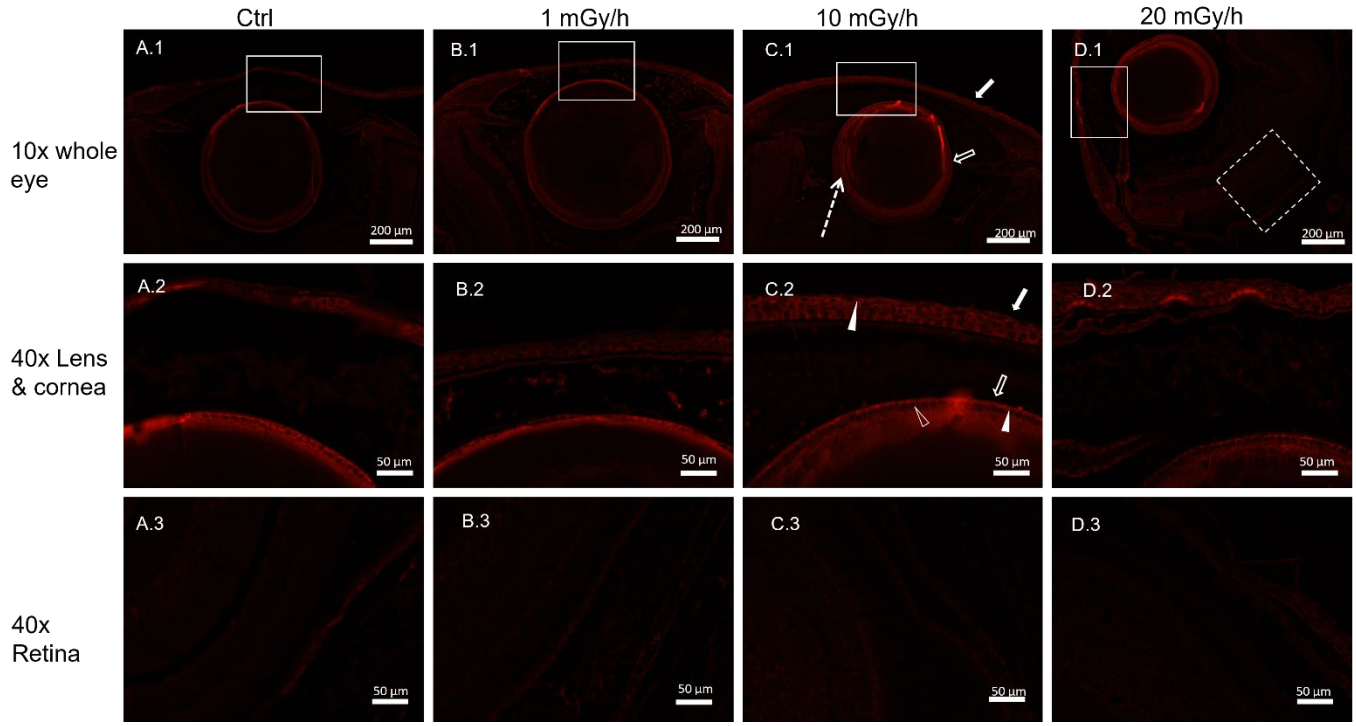

Figure 4.9 Representative Immunofluorescent images of 8OHdG. A) Control group. B) Individual exposed to γ-radiation at 1 mGy/h during embryonic development. C) Individual exposed to γ-radiation at 10 mGy/h during embryonic development. D) Individual exposed to γ-radiation at 20 mGy/h during embryonic development. Detection of 8OHdG was found in the cytoplasm (white arrowhead). No 8OHdG was detected in the nuclei (black arrowhead). Note that the sections used were taken from different depths of the eye.

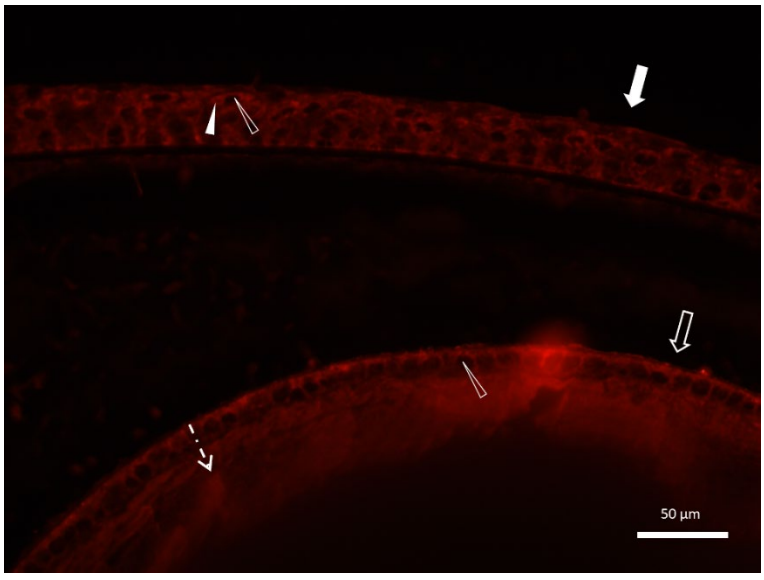

Figure 4.10 Immunofluorescent image showing 8OHdG presence in cells from the cornea (white arrow) and lens(black arrow) from fish exposed to 10 mGy/h of γ-radiation during embryonic development. The signal was most prominent in the cell cytoplasm (white arrowhead), and the nuclei were visible as black dots (black arrowhead). 8OHdG was also detected in the peripheral fiber cells (dotted arrow).

4.7 Expression of Oxoguanine DNA glycosylase 1 (OGG1)

Low-level detection of the OGG1 enzyme was found in all samples (figure 4.11). Both nuclear and cytoplasmic activity was detected in the cornea. In the lens, OGG1 expression was primarily detected in the superficial fiber cells (figure 4.12). Retinal cells showed positivity in the nuclei, although not as pronounced as in the cytoplasm of the cornea and superficial fiber cells of the lens. No significant differences between the different dose-rates were observed (figure 4.11).

The image brightness was temporarily increased with post-processing to determine the intracellular localization of antigen-antibody complexes. Images from the green channel were also processed the same way to ensure that the localized signal was not caused by autofluorescence. These images are presented in figure A.2 in the appendix.

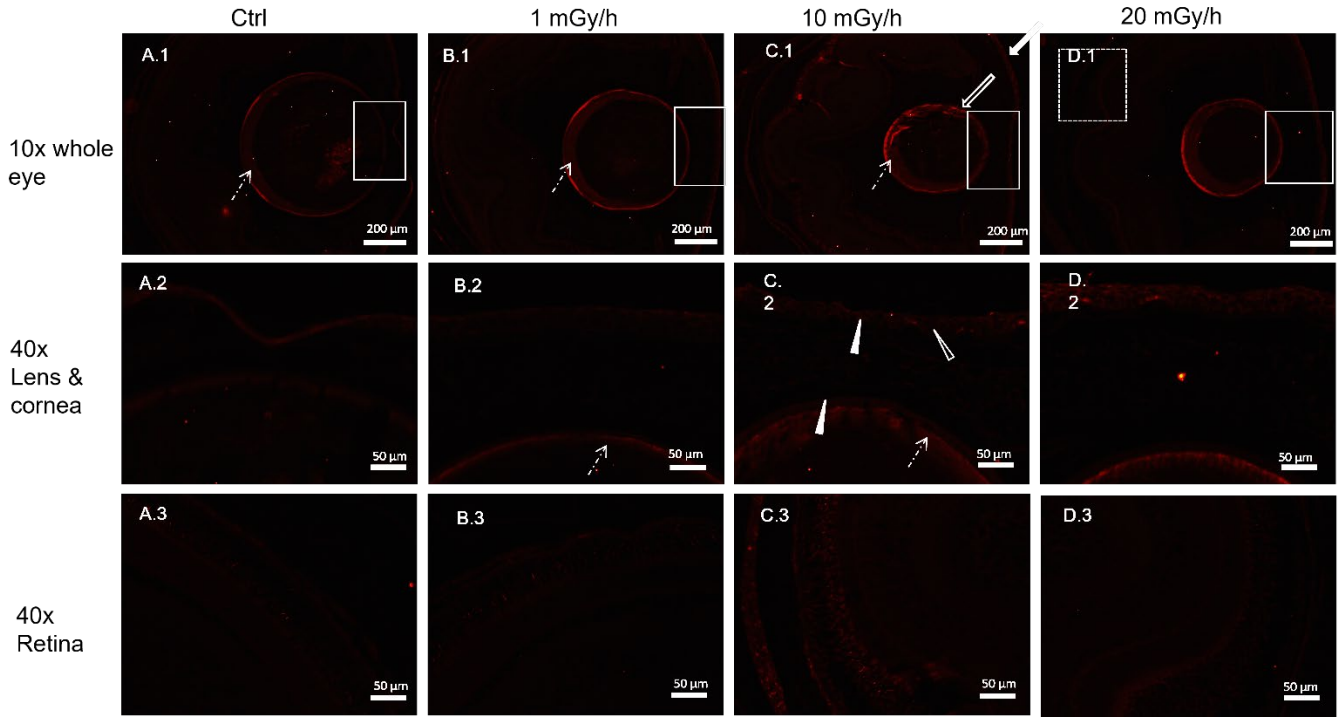

Figure 4.11 Representative selection of immunofluorescent images of OGG1 stained samples. A) Control group. B) Individual exposed to γ-radiation at 1 mGy/h during embryonic development. C) Individual exposed to γ-radiation at 10 mGy/h during embryonic development. D) Individual exposed to γ-radiation at 20 mGy/h during embryonic development. Detection was seen in the lens fiber cells (dotted arrows) at all dose-rates. Expression was found in the cytoplasm (white arrowhead) and nuclei (black arrowhead).

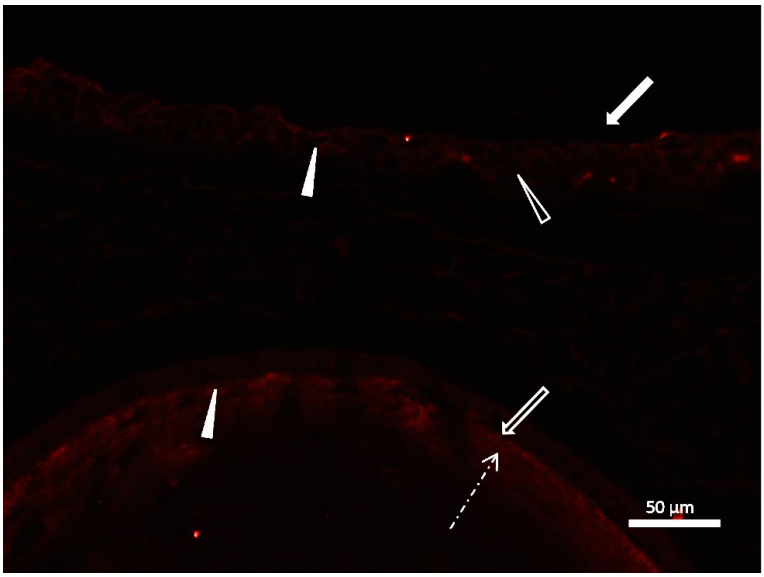

Figure 4.12 Immunofluorescent image illustrating OGG1 expression in cells from the cornea (white arrow) and lens(black arrow) from fish exposed to 10 mGy/h of γ-radiation during embryonic development. The signal was prominent in the cell cytoplasm (white arrowhead), and the nuclei were visible as black dots (black arrowhead). OGG1 was primarily detected in the superficial fiber cells (dotted arrow).

4.8 Cytoplasmic expression of apurinic endonuclease (APE1)

Apurinic endonuclease 1 (APE1) was detected in *S. salar* fry exposed to all dose-rates, including the control (figure 4.13). In the cornea, the signal was located both to the cytoplasm and cell nucleus, suggesting repair activity both in the nuclear DNA and mtDNA (figure 4.14). Images of the lens revealed APE1 activity primarily in the LECs, but some positive labeling could be seen in the superficial fiber cells. Expression was more pronounced in the nucleus of corneal cells compared to the nuclear signal from the LECs. Some levels of APE1 were also detected in the retina, mainly in the group receiving 10 mGy/h.

There seemed to be a small increase in signal intensity with increasing dose, indicating that an elevated levels of cytoplasmic APE1 could be a phenomenon related to ionizing radiation exposure in a dose-dependent manner. This was most pronounced in the 10x magnification images (figure 4.13).

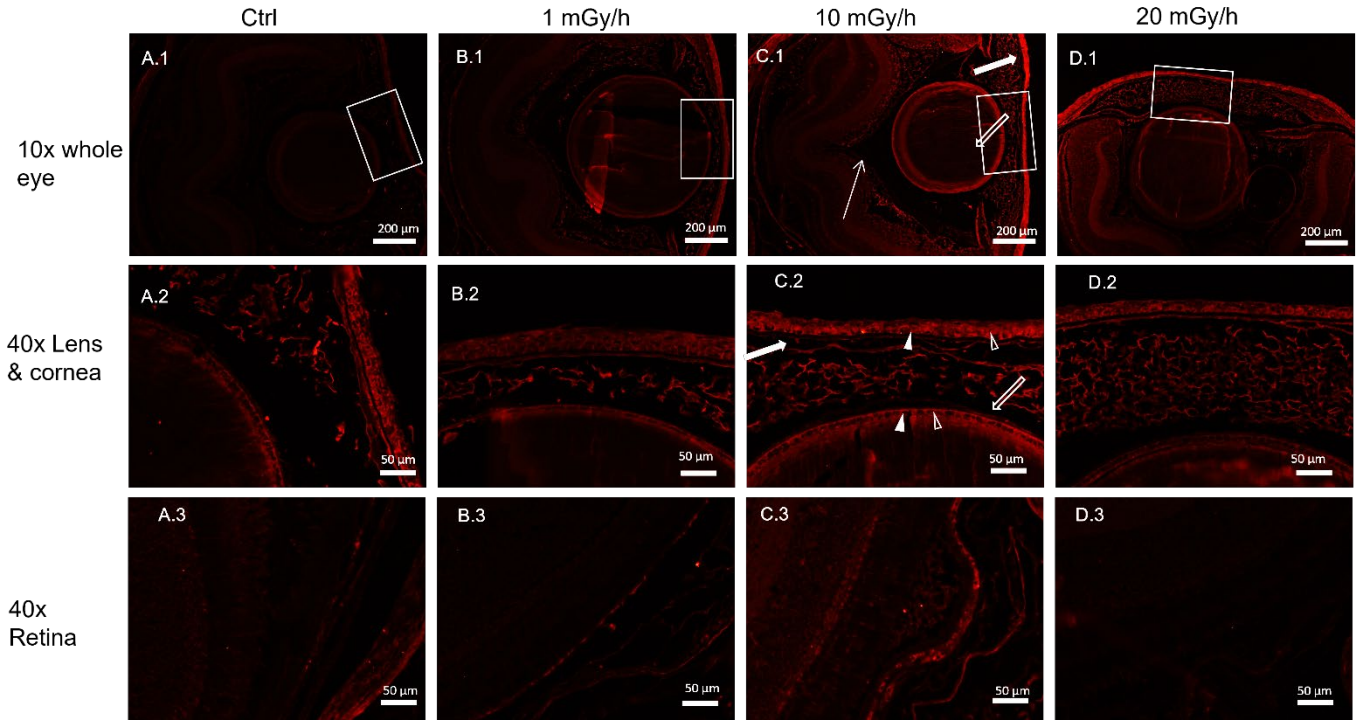

Figure 4.13 Representative selection of immunofluorescent images of APE1 stained samples. A) Control group B) Individual exposed to γ-radiation at 1 mGy/h during embryonic development. C) Individual exposed to γ-radiation at 10 mGy/h during embryonic development. D) Individual exposed to γ-radiation at 20 mGy/h during embryonic development. The signal from corneal cells was localized both in the cell cytoplasm (white arrowhead), and the nuclei (black arrowhead). The LECs expressed APE1 primarily in the cytoplasm (white arrowhead), not in the nuclei (black arrowhead). Low level expression was detected in the retina.

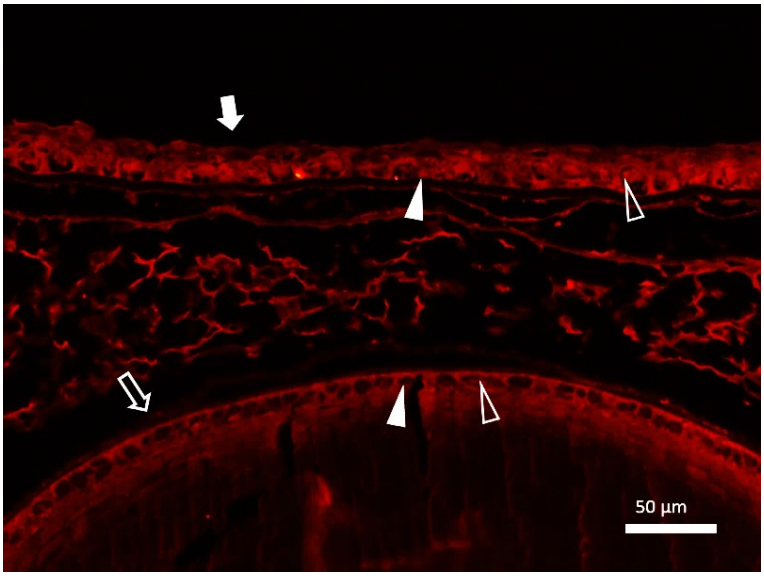

Figure 4.14 Immunofluorescent image showing APE1 expression in cells from the cornea (white arrow) and lens(black arrow) from fish exposed to 10 mGy/h of γ-radiation during embryonic development. The signal from corneal cells was localized both in the cell cytoplasm (white arrowhead), and the nuclei (black arrowhead). The LECs expressed APE1 primarily in the cytoplasm (white arrowhead), not in the nuclei (black arrowhead).

4.9 Expression of DNA-polymerase β (DNA-pol β)

DNA polymerase β (DNA-pol β)was detected at all dose-rates (figure 4.15). Expression of DNA-pol β in the cornea was primarily confined to the cell-nucleus (figure 4.16). Antigens were also detected in the lens, mainly in the cell-nucleus of the LECs, but also in the superficial fiber cells. Although the nuclear signal was most prominent, DNA-polymerase β was also detected in the cytoplasm of cells from all tissues (figure 4.16). There was also some detection in the peripheral denucleated lens-fiber cells as well as in the OFZ (figure 4.15). Detection in cell-matrix was most prominent in the LECs.

The signal intensity seems to be increasing in a dose dependent manner for some of the samples. However, time intervals between staining and imaging were longer for one series of samples, and images of this series had lower signal intensity compared to the rest. Interpretation of these images was therefore done relatively to the control of each series rather than the entire set of samples. Despite the lower signal strength, detection of DNA-polymerase β increased with increasing dose-rate, indicating elevated expression of DNA-polymerase β as a result of ionizing radiation.

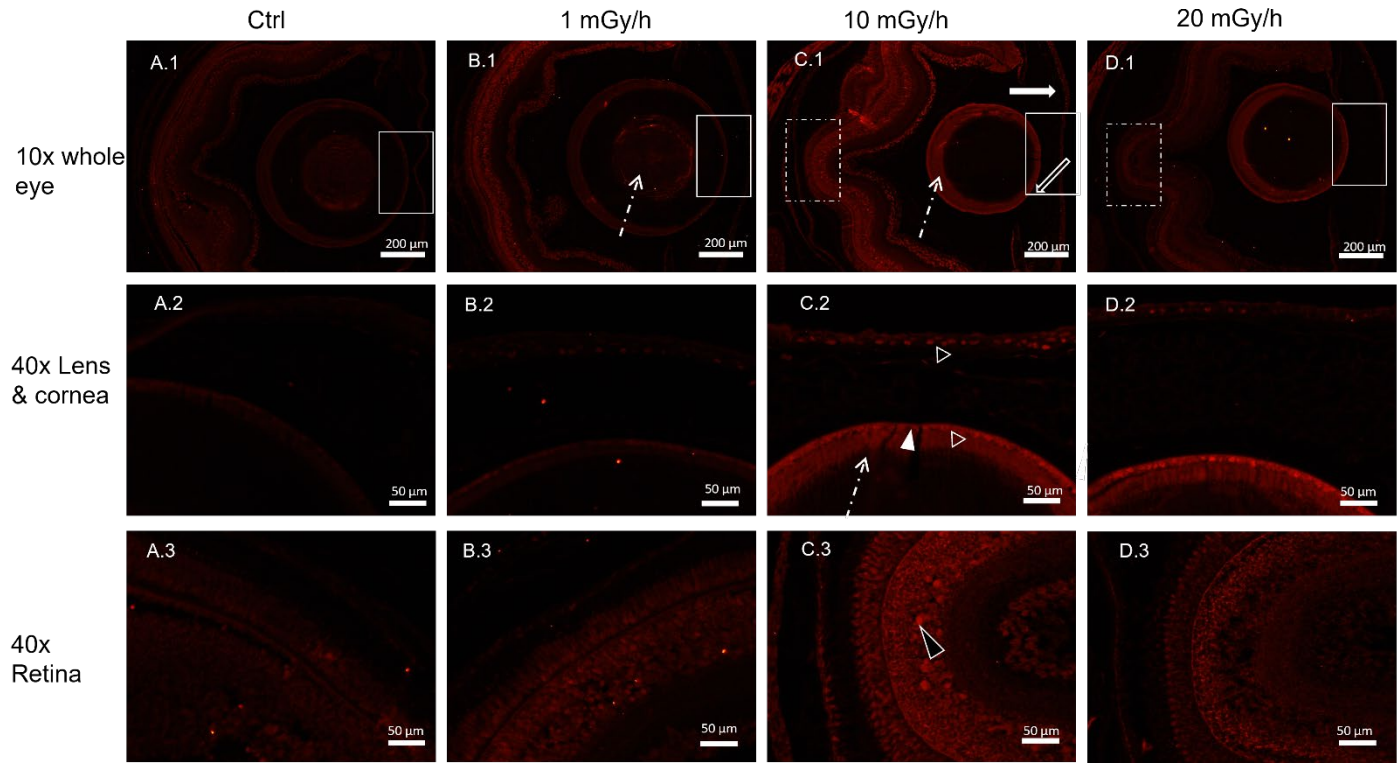

Figure 4.15 Representative immunofluorescent images of samples labeled with DNA pol-β. A) Control group. B) Individual exposed to γ-radiation at 1 mGy/h during embryonic development. C) Individual exposed to γ-radiation at 10 mGy/h during embryonic development. D) Individual exposed to γ-radiation at 20 mGy/h during embryonic development. The signal from corneal cells was localized mainly in the nuclei (black arrowhead,). A weak signal from the cytoplasm was also detected (white arrowhead). The LECs showed expression both in the cytoplasm (white arrowhead) and nuclei (black arrowhead). The enzyme was also detected in the superficial fiber cells of the lens and in the OFZ (dotted arrows). Detection in the retina was also localized in the nuclei of the cells (black arrowhead)

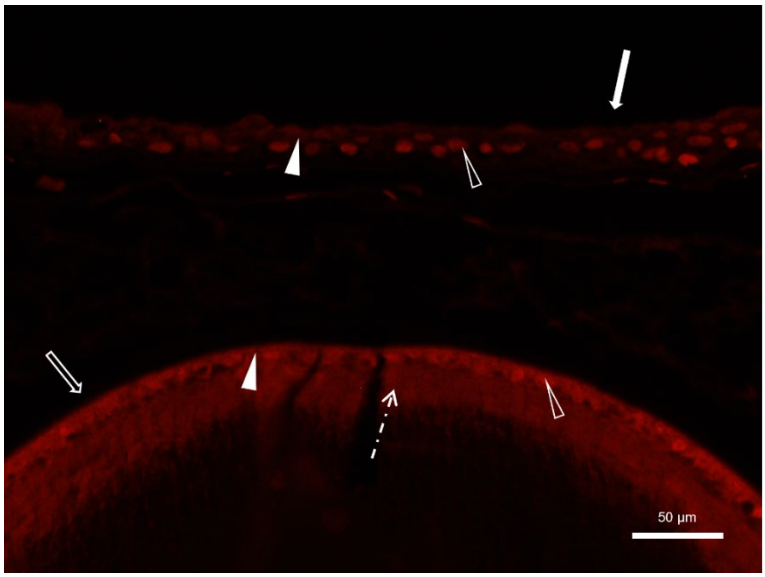

Figure 4.16 Immunofluorescent image showing DNA-polymerase β expression in cells from the cornea (white arrow) and lens(black arrow) from fish exposed to 10 mGy/h of γ-radiation during embryonic development. The signal from corneal cells was localized mainly in the nuclei (black arrowhead,) but a weak signal from the cytoplasm was also detected (white arrowhead). The LECs express DNA-polymerase β both in the cytoplasm (white arrowhead) and nuclei (black arrowhead). The enzyme was also detected in the superficial fiber cells of the lens (dotted arrow).

5. Discussion

To investigate the long-term effects on histology, development and molecular effects associated with exposure to chronic low-level γ-radiation on developing Atlantic salmon embryos, eggs were exposed at 1, 10 and 20 mGy/h for 90 days. Cell proliferation, apoptosis, autophagy, fibrosis and persistent DNA-damage were assessed by immunofluorescent staining of samples (n=14) from *S. salar* fry 3 months after exposure.

5.1 Method optimization

Method-performance was tested by enucleation of eyes from Atlantic salmon (*S. salar*) parr. Six eyes were fixed using different concentrations of paraformaldehyde for 24 and 48 hours. Dissection of the eyes was done after dehydration, but as the samples were put back on formalin while awaiting infiltration, the actual effects of different fixation-times and concentrations were no longer recognizable. Nevertheless, this extra step did not introduce any issues, and despite going from 70% EtOH directly back to formalin, no noticeable artefacts were seen. The prolonged fixation in formalin did not affect the HE staining either. As these samples were not stained with immunofluorescent markers, their reactivity is not known. However, these results showed that whole eyes may very well be dissected and fixed on formalin, and

that the method is quite robust regarding concentrations of fixative and varying levels of hydration. It must be emphasized that this was only tested for HE staining.

For some of the antibodies used in the present experiment, prolonged fixation of salmon fry did not introduce any difficulty regarding reactivity and immunofluorescent labeling. It could therefore be argued that samples may safely be stored on formalin for long periods, at least for investigation of BER related enzymes and α-SMA. However, a study by Webster et al. (2009) tested reactivity for 61 commonly used antibodies in pathology, whereas one of them was Smooth muscle actin, and found no obvious loss in reactivity for samples stored in formalin for up to 7 weeks (Webster et al., 2009). After 7 weeks, detection of antigens went down, suggesting that prolonged storage on formalin do indeed diminish reactivity, depending on the antibody. This could be a plausible explanation for the lack of reactivity seen in some of the fluorescent antibodies such as Caspase-3, Ki-67 and PCNA.

For the other antibodies used in the present study, epitope retrieval was not necessary as the images presented in the results showed strong signals and good detection of antigens in the samples. This is an important point, as it may save both time and resources in future experiments using the same antibodies. However, the antibodies with no positive detection in this experiment may have benefited from an antigen retrieval step, and this should therefore be tested in future experiments.

5.2 Histological changes

The histological differences caused by ionizing radiation were assessed by comparing sections from samples stained with HE. As presented in chapter 4.2, no obvious differences between irradiated samples and the control could be observed. Slight variations in size of the lens were seen in some images, mainly attributed to sections being obtained from different depths of the tissue. This also affected the number of visible nuclei in the peripheral fiber cells, as the differentiation of LECs takes place during migration towards the lens-center. Sections from the center of the eye would therefore have a higher proportion of fully differentiated cells compared to the shallower regions.

Interestingly, the initial underdevelopment seen in the group receiving 20 mGy/h immediately after exposure was no longer visible after a period of recovery (figure 2.5). Some of the initial difference seen immediately after exposure may partly be explained by the sample-depth from which the sections were obtained. There were bigger differences in lens size and retinal development between the 20 mGy/h and 10 mGy/h group seen in the HE images (figure 2.5) compared to the same two groups in the Hoechst images in figure 2.6. Nonetheless, there was a difference between the groups in figure 2.6 which was no longer visible 90 days after exposure. This may be explained by a period of elevated growth rates in the

samples receiving 20 mGy/h compared to the rest of the groups, implying repair and regeneration of damaged tissue during the period of recovery, as will be discussed in the subsequent chapters.

5.3 Expression of proliferative markers

The immunofluorescent markers PCNA and Ki-67 were used in this experiment to examine the long-term effect of ionizing radiation on cell proliferation. A series of reports regarding development of the lens in irradiated mice and human LECs showed that cell proliferation increased in the germinative zone of the lens after exposure to ionizing radiation (Markiewicz et al., 2015, Fujimichi and Hamada, 2014). However, none of the markers for cell proliferation used in the present study were detected in any of the samples, regardless of dose.

Given the inconsistency with previous studies, the lack of signal is most likely due to incompatibility between the antibodies and *S. salar* species. As the cells in developing tissue are naturally proliferating, one would expect to observe a basal level of expression of proliferation associated proteins such as PCNA or Ki-67 regardless of the received dose of ionizing radiation. Here, a positive control could also have been used to identify the lack of antigen-antibody recognition. Additionally, an epitope-retrieval step during tissue processing could have been beneficial.

A study performed on rabbit lenses showed that exposure to high doses of ionizing radiation reduced the lens density in the epithelial layer after exposure but induced increased cell proliferation lasting for a couple of weeks before returning to the basal level (Von Sallmann, 1952). This discovery may also be part of explaining why the difference in development seen between the histological sections of samples taken immediately after exposure and the ones taken after recovery were no longer visible. It is conceivable that there was an initial burst of proliferation during recovery that had returned to a basal level at the time of sampling.

5.4 Tissue damage and cellular responses

Autophagy and apoptosis have been reported as an effect from exposure to low-dose ionizing radiation in former studies (Chaurasia et al., 2016, Ito et al., 2005, Barrett et al., 2018). The level of autophagy and apoptosis 3 months after exposure was assessed by labeling samples from irradiated fish with markers for LC3 and caspase-3.

No elevated levels of autophagy could be reported as a long-term effect of ionizing radiationto developing embryos. As none of the images showed any pronounced positivity or difference in

expression between the exposed groups and the control, the detected levels may be attributed to the basal autophagy activity of developing cells. As autophagosomes are small compared to the cell, higher magnification images should be taken to investigate the actual number of autophagosomes, giving a better insight in the subcellular distribution and activity. Quantification of such small vesicles was impossible at the level of magnification used in this experiment given the low activity found in the cell. Also, as mentioned in chapter 4.4, there was a significant amount of autofluorescence in the retinal tissue, which required suboptimal exposure to avoid interference of autofluorescence, thus leading to false negative results.

Other studies have described autophagy as an important contributor to the differentiation and organelle loss of the LECs, and that mutations in a gene associated with recruiting LC3 amongst other proteins was involved in the formation of congenital cataracts (Chen et al., 2011, Frost et al., 2014). One would therefore expect to see some basal level of autophagy in the developing crystalline lens, especially in the LECs and in the fiber-cells outside the OFC, which was not the case in the present experiment. Another study found that ionizing radiation induced autophagy in cancer cells, which would suggest that ionizing radiation in general induce more autophagy in some cell types (Ito et al., 2005). The weak signal seen in this study was therefore most likely due to incompatibility between the species and antibody.

Mitochondrial damage is also known to induce mitophagy which is the decomposition of mitochondria (Youle and Narendra, 2011). If the positivity from labeling with APE1 and 8OHdG stems from damage and oxidative stress in the mitochondria, some mitophagy would be anticipated. Given the long recovery time, the cells might have finished the repair of damaged DNA in the nucleus and mitochondria, which would explain the absence of difference in positivity between the groups.

Images that were taken of the samples stained with LC3 in the first batch showed higher positivity than the samples stained later, despite the time between staining and imaging being longer for the first batch (results not provided). A possible explanation of this may be as simple as an error during preparation of the primary antibodies, leading to a difference in concentration between the batches. The fact that staining and imaging was performed in several batches is a limiting factor that precludes comparison between samples. Due to the low number of replicates (n=14) for each antibody, small variations between the samples made identification of variations between groups difficult Staining the samples in two batches could possibly add to this difficulty as there were twice as many stages in which errors and inconsistencies could occur.

5.5 Radiation induced fibrosis and epithelial mesenchymal transition

As fibrosis have been reported as a result from radiation therapy and general exposure to ionizing radiation (Judge et al., 2015, Nagamoto et al., 2000), α-SMA was used as a marker for detection of this response in the present study. The enzyme was expressed in all samples, and elevated expression could possibly be a phenomenon related to received dose, as presented in chapter 4.5.

Alpha smooth-muscle actin has been associated with the epithelial-mesenchymal transitioning (EMT) which is a process where epithelial cells undergo a transformation to more fibroblast like cells. Epithelial cells become more mobile during the transition and lose characteristics that are specific for epithelial cells. It has been illustrated that EMT in the LEC is associated with cataractogenesis, and that this is related to the formation of ROS in the epithelial layer in human patients with diabetic related cataracts (Wu et al., 2020, Zhang et al., 2017). Although the levels of α-SMA were slightly elevated in the individuals receiving 10 and 20 mGy/h, no sign of fibrosis was found after investigation of the HE stained samples. Fibrosis may therefore possibly occur at a later stage of development, and thus contribute to the formation of cataracts.

Due to the small sample size, ruling out any outliers interfering with observed trends was difficult. Nevertheless, discussing tendencies or differences in detection as a phenomenon rather than a quantitative study of occurrences in a population after radiation could provide valuable information.

5.6 Base Excision Repair pathway

To assess the persistent oxidative DNA damage caused by ionizing radiation, fluorescent markers were used to detect enzymes involved in the BER pathway.

5.6.1 8-hydroxy,2-deoxyguanosine (8OHdG)

Images of the 8OhdG labeled samples revealed high detection of antigens in the cytoplasm of cells from both the cornea and lens, as shown in chapter 4.6. Being a marker for oxidatively damaged DNA, one would expect the cellular localization to be the nucleus, which was unexpectedly not the case. High intensity of the signals from all groups indicated that there were little to no difference in the oxidative stress between the control and those exposed to different doses three months after exposure. All groups therefore seem to have experienced the same amount of oxidative stress at the time of sampling. A likely explanation is that the positivity seen in the images stems from oxidative stress caused by the natural metabolism in the fish. Mitochondria generate ROS as a by-product of the electron transport chain and oxidative respiration, which in turn may interact with the mtDNA that can be found in close proximity to

the membrane bound electron transport chain (Brennan and Kantorow, 2009). This interaction will then oxidize guanosine bases leading to elevated levels of 8OHdG in the mitochondria compared to the nucleus. Mitochondrial DNA is not packed around histones, unsimilar to nuclear DNA, which makes it more prone to oxidative damage. Images taken with a higher magnification level could have helped localize the intracellular distribution of the signal, confirming whether it was localized in the mitochondria or the cell-cytoplasm.

As the signal was localized in the cell cytoplasm, it may also be caused by oxidized guanosine bases found in mRNA molecules. Although the bases used in RNA are ribonucleic acids, as opposed to deoxyribonucleic acids found in the DNA, the antibodies are used to detect both oxidized bases. Some compounds have been documented to induce formation of 8-hydroxyguanosine in RNA, but no increase in 8-hydroxy-2'-deoxyguanosine in DNA from rat liver, and it is therefore a likelihood that the signal seen in this experiment is mainly from damaged RNA molecules (Hofer et al., 2006).

Interestingly, the signal from the antibodies related to oxidative damage was higher in the lens and cornea in all samples compared to the retina, regardless of received dose. As there are no blood vessels in the cornea or lens, the environment is hypoxic, meaning that the tissue needs supply of essential compounds such as oxygen from the surrounding tissue. A previous study have shown how hypoxia is important for the regulation of cell proliferation in rat epithelial cells at an older age, and that increased oxygen level also stimulated cell growth (Shui and Beebe, 2008). High levels of oxygen could therefore be important during eye development, thus explaining the elevated levels of oxidative damage in the cornea and lens compared to the retina, as the latter has a continuous supply of blood and therefore better antioxidant defense.

5.6.2 Oxoguanine glycosylase 1 (OGG1)

Staining with the human Oxoguanine glycosylase 1 showed that the antibody also had affinity to the OGG1 epitope found in *Salmo salar* despite being a human analog. This is consistent with the fact that DNA glycosylases and the BER pathway are a well conserved mechanism in all branches of life, which would suggest compatibility although with a somewhat weaker affinity (Pan et al., 2017). Weak signals in all samples call for a possible improvement of the method. A positive control could also have been used to establish a reference point for comparison.

As with the 8OHdG stained samples, OGG1 showed cytoplasmic positivity, especially in the subcapsular fiber cells of the anterior part of the lens. These findings suggest that there has been a mitochondrial expression of OGG1 rather than nuclear expression. A study regarding mitochondrial expression of

OGG1 in pancreatic cancer patients found that samples with high mitochondrial expression of OGG1 also showed high nuclear expression, something that correlates to some degree with the results from the present study (Inokuchi et al., 2020). The same study also found that the levels of 8OHdG and OGG1 were inversely correlated, and samples with high concentrations of 8OHdG had a low expression of OGG1, and vice versa. This finding correlates well with the results from the present experiment. Other studies have also stated OGG1 as an important enzyme for repair of mitochondrial DNA (Lia et al., 2018, Prakash and Doublié, 2015), which again would explain the cytoplasmic localization found in the present study.

Subcapsular location of signals may also stem from residues from previous enzymatic activity. As the LECs differentiate, organelles are digested and removed from the cells as they move toward the OFZ. If LECs have been exposed to oxidative stress while differentiating, OGG1 residues may linger in the fiber cell structures giving rise to the signal that was seen in the samples.

5.6.3 Apurinic endonuclease 1 (APE1)

Staining with APE1 gave the best overall signal strength compared to all other antibodies used in this experiment. Whether this positivity was due to binding of an actual APE1 epitope or caused by unspecific binding of the primary antibody should be addressed, as the signal was homogenously distributed between all tissues of the eye including the OFC. Negative control samples were only stained with the secondary antibody and would therefore only serve as a control for unspecific binding of the fluorescent marker to molecules naturally present in the tissue. Although the samples were permeabilized and blocked before application of the primary antibodies, serum was not from the same species as the antibody (bovine serum, rabbit and mouse antibody), and possibly less effective in blocking unspecific binding of epitopes. The half-life of APE1 is rather long compared to other enzymes, and accumulation of the enzyme over time may also be a contributing factor to the overall high positivity (Choi et al., 2016).

Cytoplasmic localization of the immunofluorescent signal is in line with mitochondrial DNA repair. Studies have reported that cytoplasmic expressed APE1 is common in cell types with high metabolism and cell proliferation, and that subcellular localization varies greatly within different cell types (Tell et al., 2005). *Salmo salar* alevin grow fast, and development of the eye is important for the ability to feed after the yolk-sac has been consumed (Bjerkås et al., 2004). High metabolism implies increased activity in the mitochondria which would further amplify the amount of oxidative stress inflicted in the cell. This would lead to elevated levels of 8OHdG and thus serve as an explanation for the elevated levels of said compound in all exposure groups and the control.

Inconsistency between expression of OGG1 and APE1 could suggest another function for the latter enzyme. Before APE1 can excise the backbone of the DNA strand, the damaged base must firstly be removed by OGG1 or another glycosylase depending on the nucleotide. Low detection of OGG1 may therefore contradict the positivity from APE1 resulting from mtDNA repair. APE1 has also been described as an important mediator of redox regulation in the cell cytoplasm, which corresponds well with the findings from this experiment (Tell et al., 2009). High levels of oxidized guanosine bases imply high levels of oxidative stress, and there is a likelihood that the activity seen from APE1 was due to its redox regulatory properties. However, a study have reported this function only in mammalian species, not in connection to fish (Georgiadis et al., 2008).

The study by Tell et al. (2009) also suggested APE1 as a central component for controlling cell proliferation and preventing cell death. Although the exact mechanisms behind this function is not well understood, a study by Vascotto et al. (2011) suggested that the redox potential of APE1 was important in mitochondria exposed to oxidative stress as it prevented apoptosis through the mitochondrial dependent pathway (Vascotto et al., 2011). Even a more recent study has described APE1 as an important endonuclease for degeneration of mitochondrial mRNA, ensuring proper functioning of mitochondrial respiration (Barchiesi et al., 2021). What is shown in both studies is consistent with the findings of the present experiment, as APE1 levels were high in the cytoplasm. Given the high levels of 8OHdG found in the cytoplasm, it seems a viable explanation that the oxidative response shown in this experiment could be attributed to the mitochondrial DNA and mRNA. It is interesting to note the lack of dose dependence in the response, as this suggests that the exposed individuals have reached homeostasis 3 months after exposure.

5.6.4 DNA polymerase β (DNA-pol β)

The nuclear localization of DNA-polymerase β fulfills the expectations of intracellular distribution. Detection in the nucleus showed that the antibody, although not from the same species, was compatible with *S. salar*, and gave good results. Interestingly, similar to APE1, this nuclear enzyme also yielded a strong cytoplasmic signal in the LECs and peripheral lens fiber cells. Sykora et al. (2017) showed in their study that DNA polymerase β is an important part of the mtDNA repair mechanism as well as the repair of nuclear DNA, and this finding supports the suggested mitochondrial damage mentioned in chapter 5.6.3 (Sykora et al., 2017). Although lens-fiber cells do not have nuclear DNA after differentiation, residues of the nucleus may persist in the cells until they reach the OFZ, thus explaining the signals found in the differentiated fiber sections (Wride, 2011). This was also the only antibody showing a pronounced and distinct signal in the OFZ, clearly separated from the peripheral fiber cells. Whether this was purely

artefactual is not known, but as the phenomenon also appeared in the control group it did not seem to correlate with exposure to ionizing radiation. However, enzyme detection in the other regions seemed to increase in individuals receiving increased exposure, suggesting a dose-response relationship between DNA repair and γ-radiation three months after exposure. Interestingly, this finding did not coincide with the intracellular localization of the other BER associated enzymes, which were predominantly located in the cytoplasm. This inconsistency may therefore emphasize a limitation of this study regarding the compatibility between antibodies and *S. salar.*

The results from this study showed expression of DNA polymerase β also in the retina, and that this response showed a higher dose dependency compared to any of the other markers in any other tissue. If this difference truly was dose dependent, appearance three months after exposure suggest that γ-radiation is likely to induce persistent damage to the DNA of the retina and thus cause genomic instability. This agrees with results from previous studies of zebrafish embryos exposed to γ-radiation (Hurem et al., 2017)

As the retina is the only tissue sustaining a continuous blood supply, bystander effects may play a role in the observed response. Clastogenic factors have been shown to be a persistent response to ionizing radiation (Morgan, 2003), and could be carried with the bloodstream from other damaged areas and deposited in the retina, causing genotoxic effects long after irradiation of the organism. Morgan et al. (2003) also points out that a lot of the clastogenic factors work by inducing free radicals. One could therefore argue that it could cause an increased level of 8OHdG in the retina, which was not the case in the results presented here.

5.7 Cataract

Cataract is, as mentioned earlier, often associated with exposure to both high and low doses of ionizing radiation (Azizova et al., 2018, Nguyen et al., 2019). Overexpression of pol-beta is correlated with the early onset of cataracts in mice (Sobol, 2003). A study investigating oxidative stress and the BER activity of lenses with age related cataracts (ARC) found significantly higher activity of the repair enzymes in the lenses from patients with ARC compared to controls (Xu et al., 2015). Different from the present study, the activity was found to be highest in the nuclei of the LECs, and 8OHdG was found in highest concentrations within the nucleus of the lens. What is brought to question in the above-mentioned study is whether the cataract cause the differences in expression or if the deficient DNA repair is causing the cataract.

If radiation induces increased cell proliferation, as is suggested in a review article from 2019, the apparent similarity in development of the lenses from the 20 mGy/h group may be a result of increased proliferation rate (Uwineza et al., 2019). The images taken immediately after exposure (figure 2.5 and 2.6) showed a clear underdevelopment of the eye compared to the groups receiving lower doses, but the difference was no longer observable after 3 months of recovery. The tissue in the 20 mGy/h group must therefore have developed more rapidly than the other groups, before stabilizing at a normal growth rate. This is in line with what is mentioned in the article by Uwineza et al. (2019), where the increase in proliferation only lasted for a couple of weeks. An increase in proliferation would also mean an increase in metabolic activity and especially an increase in mitochondrial activity, possibly giving rise to an increased production of ROS, and possibly contributing to cataract development in the future (Bjerkås et al., 2004, Bjerkås et al., 1996).

Lens crystalline proteins are easily oxidized if exposed to oxidative stress, and will readily aggregate resulting in lens opacification (Williams, 2008). As the fish lens has an even higher concentration of crystalline proteins than human lenses, one would expect the lenses of fish to be even more susceptible to formation of cataracts caused by oxidation of the crystalline proteins. The high levels of oxidized guanosine in the lens epithelium and outside the organelle free zone found in all groups, including the control, suggests a high basal level of oxidative stress in the lens. A study on cataracts in salmon and trout found that the salmon used in the experiment had large individual differences in the glutathione levels of the lens (Remø et al., 2017). As glutathione is involved in the antioxidant defense, insufficient levels of the enzyme may lead to increased oxidative damage and thus increasing the risk of cataracts. This individual difference in glutathione may also help explain the variations within each group used in the present study, adding to the difficulty of finding the effects caused by radiation dose. The same study also described a high prevalence of cataracts in salmon reared under optimal conditions. If the endpoints used in the present study are indeed related to the formation of lens-opacities, the findings are consistent with what is described in the study by Remø et al. (2017).

5.8 Challenges and suggestions for further work

To investigate the mechanisms of radiation induced stress and the development of the eye, analysis of the BER enzymes should be carried out immediately after exposure as a means to compare the long-term effects and changes in the enzymatic activity and expression. Also, investigation of the crystalline proteins present in the lens should be conducted to look for differences in protein concentrations that may eventually lead to formation of cataracts.

Investigation of the late-stage development of cataracts in *Salmo Salar* due to exposure of ionizing radiation could also be of interest. Although coming at a considerable cost, it could be worthwhile as other studies have suggested a high prevalence of cataracts in *S. Salar* reared under normal conditions (Bjerkås et al., 2004, Remø et al., 2017). By rearing the exposed individuals under normal conditions and observing their development to post-smolt life stage and transition to salt water could reveal late life effects and formation of cataracts. Development of cataracts may take months or years and may therefore not be visible at the time of sampling in this experiment. It is known that the transition from fresh to salt water is a highly sensitive life-stage for *S. salar,* and mortality numbers etc. could reveal possible effects on viability from chronic exposure to ionizing radiation. As mentioned earlier, osmotic cataracts is known to occur at this stage, and investigating the impact from ionizing radiation on this phenomenon could be of interest (Bjerkås et al., 2004).

The immunohistochemical methodology could potentially be improved by further experimentation and optimization of fixation procedures and different blocking solutions to enhance selectivity of antibodies. Studies have showed that different antibodies require different fixation procedures, and an optimized method may therefore lead to more quantifiable results (Arnold et al., 1996, Nietner et al., 2012, Howat and Wilson, 2014). However, as prolonged fixation is known to reduce reactivity (Webster et al., 2009), this cannot be ruled out as a possible explanation to the lack of signal from some of the antibodies. Formalin could therefore be used as a fixative when repeating the experiment, but the samples should be processed and analyzed preferably withing the 7 day limit as proposed by Webster et al. (2009), alternatively stored on ethanol for longer periods.

Strong signals may be a consequence of erroneously dilution of antibodies, leading to a high degree of non-specific binding due to excessively high concentration of antibodies. Time of incubation could also have affected this, but as other antibodies were not overly positive, false positives most likely results from high concentrations of antibodies. Blocking serum should preferably be from the same animal species as the secondary antibody, or from that of the samples, in this case *Salmo salar*. If the antibodies of the serum do not recognize the non-specific epitopes, the primary antibodies may bind instead, causing non-specific binding (Kim et al., 2016).

Quantification of signal intensity is another challenge uncovered by this experiment. Increasing exposure of images to get a background reading, and then subtract the background from the fluorescent channel to get the overall difference could yield more quantifiable results (Noller et al., 2016). The levels of autofluorescence were not homogenously distributed throughout the different tissues of the eye, and the exposure may therefore be overcompensated in some parts of the eye. Autofluorescence may have

different intensities between different channels as the light has different wavelengths, posing another challenge to the exposure-adjustment.

Better quantification of signal is also crucial for producing more statistically significant results. Sample-variations within the groups also cause a difficulty in finding statistically significant differences and increasing the number of replicates could improve this problem. Quantification of immunohistochemical data is done by scoring, and the data is therefore categorical, thus a Mann-Whitney U test is recommended for statistical testing. As the samples were stained in different batches, all observations could not be used when comparing the data, and despite having 4 replicates for each group, n=3 was effectively the largest amount of samples appropriate for comparison. Increasing the number of replicates for each group and staining all samples in the same batch (at least each marker) could help identify outliers and thus facilitate the identification of variance. As there were 4 groups receiving different treatments, using 6 replicates from each group would ensure a higher number of observations compared to treatments and leaving room for outliers and artefacts. This way, variations within the group can be compared with variations between different exposures.

As the quantification was done subjectively, small nuances might be overlooked and could therefore contribute to great differences in scoring of the signal strength. To back up observations of signal detection, a chemical analysis of enzyme concentration or 8OHdG concentration could be performed to have a better quantification of actual enzyme or epitope concentration in the samples.

6. Conclusion

The long-term effects of low-dose γ-radiation (1, 10 and 20 mGy/h) on eye development of Atlantic salmon alevin were assessed with immunofluorescent and histochemical analysis. No histological effects could be observed 3 months after exposure, and individuals receiving doses at 20 mGy/h showed similar development to the other groups, probably due to an increased growth-rate for a short period right after exposure. Thus, the hypothesis that chronic exposure to γ-radiation leads to persistent deformities and tissue damage could not be confirmed.

None of the markers used for investigation of cell proliferation or cell death yielded positive results, most likely due to incompatibility between the antibodies used and *Salmo salar* as a species. On the other and, some of the markers used to investigate molecular effects showed a tendency for a dose-response relationship between exposure and outcome. Although not statistically documented, this could be seen as elevated levels of DNA-polymerase β in the nuclei with increasing dose, suggesting persistent DNA damage as a response to ionizing radiation. Also, increased expression of α-SMA as a response to higher dose was observed and could be a phenomenon related to chronic exposure to γ-radiation, despite no detectable fibrosis in any tissue of the eye. This finding also suggests elevated expression of α-SMA as a persistent response to γ-radiation exposure. Additionally, the results supports the hypothesis that human antibodies can be used in fish studies, at least for some of the antigens used.

Analysis of the BER enzymes present in the samples showed low levels of detection in the nucleus, thus suggesting no persistent damage to the DNA three months after exposure. Most enzymatic activity was found in the cytoplasm, and detection was therefore attributed to mtDNA and RNA damage. However, DNA-polymerase β was mainly located in the nuclei, showing elevated levels of expression as a response to low-dose γ-radiation.

No findings directly related to clinical cataracts was acquired in the experiment. Nonetheless, indications of mechanisms related to the development of cataracts such as periodically elevated growth-rate, detection of markers for fibrotic tissue and detection of oxidative damage in the lens and LECs showed increasing tendencies after exposure to γ-radiation. Thus, the hypothesized relationship between increased levels of cataract associated molecular markers was to some degree confirmed. However, the lack of statistical confirmation and clinical documentation suggests that more research on this topic is needed.

7. References

ABDULHUSSEIN, D., KANDA, M., AAMIR, A., MANZAR, H., YAP, T. E. & CORDEIRO, M. F. 2021. Chapter Nine - Apoptosis in health and diseases of the eye and brain. *In:* DONEV, R. (ed.) *Advances in Protein Chemistry and Structural Biology.* Academic Press.

AINSBURY, E. A., BARNARD, S., BRIGHT, S., DALKE, C., JARRIN, M., KUNZE, S., TANNER, R., DYNLACHT, J. R., QUINLAN, R. A., GRAW, J., KADHIM, M. & HAMADA, N. 2016. Ionizing radiation induced cataracts: Recent biological and mechanistic developments and perspectives for future research. *Mutat Res,* 770**,** 238-261.

AL-MAYAH, A., BRIGHT, S., CHAPMAN, K., IRONS, S., LUO, P., CARTER, D., GOODWIN, E. & KADHIM, M. 2015. The non-targeted effects of radiation are perpetuated by exosomes. *Mutat Res,* 772**,** 38-45.

AMIRABADI, E., SALIMI, M., GHAL-EH, N., ETAATI, G. & ASADI, H. 2013. Study of Neutron and Gamma Radiation Protective Shield. *International Journal of Innovation and Applied Studies,* 4**,** 1079-1085.

ARNOLD, M. M., SRIVASTAVA, S., FREDENBURGH, J., STOCKARD, C. R., MYERS, R. B. & GRIZZLE, W. E. 1996. Effects of Fixation and Tissue Processing on Immunohistochemical Demonstration of Specific Antigens. *Biotechnic & Histochemistry,* 71**,** 224-230.

AZIZOVA, T. V., HAMADA, N., GRIGORYEVA, E. S. & BRAGIN, E. V. 2018. Risk of various types of cataracts in a cohort of Mayak workers following chronic occupational exposure to ionizing radiation. *European Journal of Epidemiology,* 33**,** 1193-1204.

AZZAM, E. I., JAY-GERIN, J. P. & PAIN, D. 2012. Ionizing radiation-induced metabolic oxidative stress and prolonged cell injury. *Cancer Lett,* 327**,** 48-60.

BARCHIESI, A., BAZZANI, V., JABCZYNSKA, A., BOROWSKI, L. S., OELJEKLAUS, S., WARSCHEID, B., CHACINSKA, A., SZCZESNY, R. J. & VASCOTTO, C. 2021. DNA Repair Protein APE1 Degrades Dysfunctional Abasic mRNA in Mitochondria Affecting Oxidative Phosphorylation. *Journal of Molecular Biology,* 433**,** 167125.

BARNARD, S. G. R., MCCARRON, R., MANCUSO, M., DE STEFANO, I., PAZZAGLIA, S., PAWLICZEK, D., DALKE, C. & AINSBURY, E. A. 2021. Radiation-induced DNA Damage and Repair in Lens Epithelial Cells of both Ptch1(+/-) and Ercc2(+/-) Mutated Mice. *Radiat Res*.

BARNARD, S. G. R., MCCARRON, R., MOQUET, J., QUINLAN, R. & AINSBURY, E. 2019. Inverse dose-rate effect of ionising radiation on residual 53BP1 foci in the eye lens. *Sci Rep,* 9**,** 10418.

BARNARD, S. G. R., MOQUET, J., LLOYD, S., ELLENDER, M., AINSBURY, E. A. & QUINLAN, R. A. 2018. Dotting the eyes: mouse strain dependency of the lens epithelium to low dose radiation-induced DNA damage. *Int J Radiat Biol,* 94**,** 1116-1124.

BARRETT, C., HELLICKSON, I., BEN-AVI, L., LAMB, D., KRAHENBUHL, M. & CERVENY, K. L. 2018. Impact of Low-level Ionizing Radiation on Cell Death During Zebrafish Embryonic Development. *Health Phys,* 114**,** 421-428.

BEARD, W. A. & WILSON, S. H. 2014. Structure and Mechanism of DNA Polymerase β. *Biochemistry,* 53**,** 2768-2780.

BEJARANO-ESCOBAR, R., BLASCO, M., MARTÍN-PARTIDO, G. & FRANCISCO-MORCILLO, J. 2014. Molecular characterization of cell types in the developing, mature, and regenerating fish retina. *Reviews in Fish Biology and Fisheries,* 24**,** 127-158.

BERTHOUD, V. M. & BEYER, E. C. 2009. Oxidative stress, lens gap junctions, and cataracts. *Antioxid Redox Signal,* 11**,** 339-53.

BJERKÅS, E., HOLST, J. C. & BJERKÅS, I. Cataract in farmed and wild Atlantic salmon (Salmo salar L.). 2004.

BJERKÅS, E., WAAGBØ, R., SVEIER, H., BRECK, O., BJERKÅS, L., BJORNESTAD, E. & MAAGE, A. 1996. Cataract Development in Atlantic Salmon (Salmo salar L) in Fresh Water. *Acta Veterinaria Scandinavica,* 37**,** 351-360.

BOICE, J. D., HELD, K. D. & SHORE, R. E. 2019. Radiation epidemiology and health effects following low-level radiation exposure. *Journal of Radiological Protection,* 39**,** S14-S27.

BRENNAN, L. A. & KANTOROW, M. 2009. Mitochondrial function and redox control in the aging eye: Role of MsrA and other repair systems in cataract and macular degenerations. *Experimental Eye Research,* 88**,** 195-203.

BRIAN, G. & TAYLOR, H. 2001. Cataract blindness--challenges for the 21st century. *Bull World Health Organ,* 79**,** 249-56.

CHAURASIA, M., BHATT, A. N., DAS, A., DWARAKANATH, B. S. & SHARMA, K. 2016. Radiation-induced autophagy: mechanisms and consequences. *Free Radical Research,* 50**,** 273-290.

CHEN, J., MA, Z., JIAO, X., FARISS, R., KANTOROW, L., WANDA, KANTOROW, M., PRAS, E., FRYDMAN, M., PRAS, E., RIAZUDDIN, S., RIAZUDDIN, A., S. & HEJTMANCIK, F., J. 2011. Mutations in FYCO1 Cause Autosomal-Recessive Congenital Cataracts. *The American Journal of Human Genetics,* 88**,** 827-838.

CHENG, K. C., CAHILL, D. S., KASAI, H., NISHIMURA, S. & LOEB, L. A. 1992. 8-Hydroxyguanine, an abundant form of oxidative DNA damage, causes G-T and A-C substitutions. *Journal of Biological Chemistry,* 267**,** 166-172.

CHOI, S., JOO, H. K. & JEON, B. H. 2016. Dynamic Regulation of APE1/Ref-1 as a Therapeutic Target Protein. *Chonnam Medical Journal,* 52**,** 75.

CHOPPIN, G., LILJENZIN, J.-O., RYDBERG, J. & EKBERG, C. 2014. *Radiochemistry and nuclear chemistry,* Amsterdam, Elsevier.

CLAYCAMP, H. G., OKLADNIKOVA, N. D., AZIZOVA, T. V., BELYAEVA, Z. D., BOECKER, B. B., PESTERNIKOVA, V. S., SCOTT, B. R., SHEKHTER-LEVIN, S., SUMINA, M. V., SUSSMAN, N. B., TEPLYAKOV, II & WALD, N. 2000. Deterministic effects from occupational radiation exposures in a cohort of Mayak PA workers: data base description. *Health physics,* 79**,** 48-54.

COONS, A. H., CREECH, H. J. & JONES, N. R. B., ERNST 1942. The Demonstration of Pneumococcal Antigen in Tissues by the Use of Fluorescent Antibody. *The Journal of Immunology,* 45**,** 159-170.

DAHM, R., SCHONTHALER, H. B., SOEHN, A. S., VAN MARLE, J. & VRENSEN, G. F. 2007. Development and adult morphology of the eye lens in the zebrafish. *Exp Eye Res,* 85**,** 74-89.

DAHM, R., VAN MARLE, J., QUINLAN, R. A., PRESCOTT, A. R. & VRENSEN, G. F. J. M. 2011. Homeostasis in the vertebrate lens: mechanisms of solute exchange. *Philosophical Transactions of the Royal Society B: Biological Sciences,* 366**,** 1265-1277.

DALKE, C., NEFF, F., BAINS, S. K., BRIGHT, S., LORD, D., REITMEIR, P., ROSSLER, U., SAMAGA, D., UNGER, K., BRASELMANN, H., WAGNER, F., GREITER, M., GOMOLKA, M., HORNHARDT, S., KUNZE, S., KEMPF, S. J., GARRETT, L., HOLTER, S. M., WURST, W., ROSEMANN, M., AZIMZADEH, O., TAPIO, S., AUBELE, M., THEIS, F., HOESCHEN, C., SLIJEPCEVIC, P., KADHIM, M., ATKINSON, M., ZITZELSBERGER, H., KULKA, U. & GRAW, J. 2018. Lifetime study in mice after acute low-dose ionizing radiation: a multifactorial study with special focus on cataract risk. *Radiat Environ Biophys,* 57**,** 99-113.

DESOUKY, O., DING, N. & ZHOU, G. 2015. Targeted and non-targeted effects of ionizing radiation. *Journal of Radiation Research and Applied Sciences,* 8**,** 247-254.

ELMORE, S. 2007. Apoptosis: A Review of Programmed Cell Death. *Toxicologic Pathology,* 35**,** 495-516.

EPPERLY, M. W., BAHARY, N., QUADER, M., DEWALD, V. & GREENBERGER, J. S. 2012. The zebrafish--Danio rerio--is a useful model for measuring the effects of small-molecule mitigators of late effects of ionizing irradiation. *In vivo (Athens, Greece),* 26**,** 889-897.

FROST, L. S., MITCHELL, C. H. & BOESZE-BATTAGLIA, K. 2014. Autophagy in the eye: Implications for ocular cell health. *Experimental Eye Research,* 124**,** 56-66.

FUJIMICHI, Y. & HAMADA, N. 2014. Ionizing Irradiation Not Only Inactivates Clonogenic Potential in Primary Normal Human Diploid Lens Epithelial Cells but Also Stimulates Cell Proliferation in a Subset of This Population. *PLoS ONE,* 9**,** e98154.

GABBIANI, G. 1992. The biology of the myofibroblast. *Kidney Int,* 41**,** 530-2.

GEORGIADIS, M. M., LUO, M., GAUR, R. K., DELAPLANE, S., LI, X. & KELLEY, M. R. 2008. Evolution of the redox function in mammalian apurinic/apyrimidinic endonuclease. *Mutation Research/Fundamental and Molecular Mechanisms of Mutagenesis,* 643**,** 54-63.

GLICK, D., BARTH, S. & MACLEOD, K. F. 2010. Autophagy: cellular and molecular mechanisms. *The Journal of Pathology,* 221**,** 3-12.

GORODILOV, Y. N. 1996. Description of the early ontogeny of the Atlantic salmon, Salmo salar, with a novel system of interval (state) identification. *Environmental Biology of Fishes,* 47**,** 109-127.

GREILING, T., AOSE, M. & CLARK, J. 2009. Cell Fate and Differentiation of the Developing Ocular Lens. *Investigative ophthalmology & visual science,* 51**,** 1540-6.

HAMADA, N. 2017. Ionizing radiation sensitivity of the ocular lens and its dose rate dependence. *Int J Radiat Biol,* 93**,** 1024-1034.

HAMADA, N., AZIZOVA, T. V. & LITTLE, M. P. 2020. An update on effects of ionizing radiation exposure on the eye. *Br J Radiol,* 93**,** 20190829.

HAMADA, N. & FUJIMICHI, Y. 2014. Classification of radiation effects for dose limitation purposes: history, current situation and future prospects. *Journal of Radiation Research,* 55**,** 629-640.

HAROCOPOS, G. J., ALVARES, K. M., KOLKER, A. E. & BEEBE, D. C. 1998. Human age-related cataract and lens epithelial cell death. *Invest Ophthalmol Vis Sci,* 39**,** 2696-706.

HAVAKI, S., KOTSINAS, A., CHRONOPOULOS, E., KLETSAS, D., GEORGAKILAS, A. & GORGOULIS, V. G. 2015. The role of oxidative DNA damage in radiation induced bystander effect. *Cancer Letters,* 356**,** 43-51.

HILLENMAYER, A., WERTHEIMER, C. M., KASSUMEH, S., VON STUDNITZ, A., LUFT, N., OHLMANN, A., PRIGLINGER, S. & MAYER, W. J. 2020. Evaluation of posterior capsule

opacification of the Alcon Clareon IOL vs the Alcon Acrysof IOL using a human capsular bag model. *BMC Ophthalmology,* 20.

HOFER, T., SEO, A. Y., PRUDENCIO, M. & LEEUWENBURGH, C. 2006. A method to determine RNA and DNA oxidation simultaneously by HPLC-ECD: greater RNA than DNA oxidation in rat liver after doxorubicin administration. *Biological Chemistry,* 387**,** 103-111.

HOWAT, W. J. & WILSON, B. A. 2014. Tissue fixation and the effect of molecular fixatives on downstream staining procedures. *Methods (San Diego, Calif.),* 70**,** 12-19.

HUREM, S., MARTÍN, L. M., BREDE, D. A., SKJERVE, E., NOURIZADEH-LILLABADI, R., LIND, O. C., CHRISTENSEN, T., BERG, V., TEIEN, H.-C., SALBU, B., OUGHTON, D. H., ALESTRÖM, P. & LYCHE, J. L. 2017. Dose-dependent effects of gamma radiation on the early zebrafish development and gene expression. *PLOS ONE,* 12**,** e0179259.

ICRP 2012a. ICRP Publication 119: Compendium of dose coefficients based on ICRP Publication 60. *Ann ICRP,* 41 Suppl 1**,** 1-130.

ICRP 2012b. ICRP Statement on Tissue Reactions and Early and Late Effects of Radiation in Normal Tissues and Organs — Threshold Doses for Tissue Reactions in a Radiation Protection Context. *Annals of the ICRP,* 41**,** 1-322.

INOKUCHI, S., ITOH, S., YOSHIZUMI, T., YUGAWA, K., YOSHIYA, S., TOSHIMA, T., TAKEISHI, K., IGUCHI, T., SANEFUJI, K., HARADA, N., SUGIMACHI, K., IKEGAMI, T., KOHASHI, K., TAGUCHI, K., YONEMASU, H., FUKUZAWA, K., ODA, Y. & MORI, M. 2020. Mitochondrial expression of the DNA repair enzyme OGG1 improves the prognosis of pancreatic ductal adenocarcinoma. *Pancreatology,* 20**,** 1175-1182.

ITO, H., DAIDO, S., KANZAWA, T., KONDO, S. & KONDO, Y. 2005. Radiation-induced autophagy is associated with LC3 and its inhibition sensitizes malignant glioma cells. *International Journal of Oncology,* 26**,** 1401-1410.

JOUSSEN, A. M., HUPPERTZ, B., KOCH, H. R., KERNERT, N., CAMPHAUSEN, K., SCHLOSSER, K., FOERSTER, A. M., KRUSE, F. E., LAPPAS, A. & KIRCHHOF, B. 2001. Low-dose-rate ionizing irradiation for inhibition of secondary cataract formation. *Int J Radiat Oncol Biol Phys,* 49**,** 817-25.

JUDGE, J. L., OWENS, K. M., POLLOCK, S. J., WOELLER, C. F., THATCHER, T. H., WILLIAMS, J. P., PHIPPS, R. P., SIME, P. J. & KOTTMANN, R. M. 2015. Ionizing radiation induces myofibroblast differentiation via lactate dehydrogenase. *Am J Physiol Lung Cell Mol Physiol,* 309**,** L879-87.

KADHIM, M., SALOMAA, S., WRIGHT, E., HILDEBRANDT, G., BELYAKOV, O. V., PRISE, K. M. & LITTLE, M. P. 2013. Non-targeted effects of ionising radiation--implications for low dose risk. *Mutat Res,* 752**,** 84-98.

KAGLYAN, A. Y., GUDKOV, D. I., KIREYEV, S. I., YURCHUK, L. P. & GUPALO, Y. A. 2019. Fish of the Chernobyl Exclusion Zone: Modern Levels of Radionuclide Contamination and Radiation Doses. 55**,** 81-99.

KALLURI, R. & WEINBERG, R. A. 2009. The basics of epithelial-mesenchymal transition. *Journal of Clinical Investigation,* 119**,** 1420-1428.

KAMSTRA, J. H., HUREM, S., MARTIN, L. M., LINDEMAN, L. C., LEGLER, J., OUGHTON, D., SALBU, B., BREDE, D. A., LYCHE, J. L. & ALESTROM, P. 2018. Ionizing radiation induces transgenerational effects of DNA methylation in zebrafish. *Sci Rep,* 8**,** 15373.

KIM, S.-W., ROH, J. & PARK, C.-S. 2016. Immunohistochemistry for Pathologists: Protocols, Pitfalls, and Tips. *Journal of Pathology and Translational Medicine,* 50**,** 411-418.

KINO, K., HIRAO-SUZUKI, M., MORIKAWA, M., SAKAGA, A. & MIYAZAWA, H. 2017. Generation, repair and replication of guanine oxidation products. *Genes and Environment,* 39.

KOZŁOWSKI, T. M. L. U. 2018. *Fish Lenses : Anatomy and Optics.* PhD, Lund University, Faculty of Science, Department of Biology.

KROKAN, H. E. & BJORAS, M. 2013. Base Excision Repair. *Cold Spring Harbor Perspectives in Biology,* 5**,** a012583-a012583.

KRYSHEV, A. I. & SAZYKINA, T. G. 2012. Comparative analysis of doses to aquatic biota in water bodies impacted by radioactive contamination. *Journal of Environmental Radioactivity,* 108**,** 9-14.

LALL, R., GANAPATHY, S., YANG, M., XIAO, S., XU, T., SU, H., SHADFAN, M., ASARA, J. M., HA, C. S., BEN-SAHRA, I., MANNING, B. D., LITTLE, J. B. & YUAN, Z.-M. 2014. Low-dose radiation exposure induces a HIF-1-mediated adaptive and protective metabolic response. *Cell Death & Differentiation,* 21**,** 836-844.

LAUBER, K., ERNST, A., ORTH, M., HERRMANN, M. & BELKA, C. 2012. Dying cell clearance and its impact on the outcome of tumor radiotherapy. *Front Oncol,* 2**,** 116.

LEREBOURS, A., GUDKOV, D., NAGORSKAYA, L., KAGLYAN, A., RIZEWSKI, V., LESHCHENKO, A., BAILEY, E. H., BAKIR, A., OVSYANIKOVA, S., LAPTEV, G. & SMITH, J. T. 2018. Impact of Environmental Radiation on the Health and Reproductive Status of Fish from Chernobyl. *Environ Sci Technol,* 52**,** 9442-9450.

LI, W. C., KUSZAK, J. R., DUNN, K., WANG, R. R., MA, W. C., WANG, G. M., SPECTOR, A., LEIB, M., COTLIAR, A. M., WEISS, M., ESPY, J., HOWARD, G., FARRIS, R. L., AURAN, J., DONN, A., HOFELDT, A., MACKAY, C., MERRIAM, J., MITTL, R. & SMITH, T. R. 1995. Lens Epithelial-Cell Apoptosis Appears to Be a Common Cellular Basis for Non-Congenital Cataract Development in Humans and Animals. *Journal of Cell Biology,* 130**,** 169-181.

LIA, D., REYES, A., ARAÚJO DE MELO CAMPOS, J. T., PIOLOT, T., BAIJER, J., RADICELLA, J. P. & CAMPALANS, A. 2018. Mitochondrial maintenance under oxidative stress depends on mitochondrial but not nuclear α isoform of OGG1. *Journal of Cell Science,* 131**,** jcs213538.

LIANG, F.-Q. & GODLEY, B. F. 2003. Oxidative stress-induced mitochondrial DNA damage in human retinal pigment epithelial cells: a possible mechanism for RPE aging and age-related macular degeneration. *Experimental Eye Research,* 76**,** 397-403.

LICHTMAN, J. W. & CONCHELLO, J.-A. 2005. Fluorescence microscopy. *Nature Methods,* 2**,** 910-919.

LINDEMAN, L. C., KAMSTRA, J. H., BALLANGBY, J., HUREM, S., MARTIN, L. M., BREDE, D. A., TEIEN, H. C., OUGHTON, D. H., SALBU, B., LYCHE, J. L. & ALESTROM, P. 2019. Gamma radiation induces locus specific changes to histone modification enrichment in zebrafish and Atlantic salmon. *PLoS One,* 14**,** e0212123.

LITTLE, M. P., WAKEFORD, R., TAWN, E. J., BOUFFLER, S. D. & BERRINGTON DE GONZALEZ, A. 2009. Risks Associated with Low Doses and Low Dose Rates of Ionizing Radiation: Why Linearity May Be (Almost) the Best We Can Do. *Radiology,* 251**,** 6-12.

MACQUEEN, D. J., ROBB, D. H. F., OLSEN, T., MELSTVEIT, L., PAXTON, C. G. M. & JOHNSTON, I. A. 2008. Temperature until the 'eyed stage' of embryogenesis programmes the growth trajectory and muscle phenotype of adult Atlantic salmon. *Biology Letters,* 4**,** 294-298.

MAHLER, B., CHEN, Y., FORD, J., THIEL, C., WISTOW, G. & WU, Z. 2013. Structure and Dynamics of the Fish Eye Lens Protein, γM7-Crystallin. *Biochemistry,* 52**,** 3579-3587.

MARKIEWICZ, E., BARNARD, S., HAINES, J., COSTER, M., VAN GEEL, O., WU, W., RICHARDS, S., AINSBURY, E., ROTHKAMM, K., BOUFFLER, S. & QUINLAN, R. A. 2015. Nonlinear ionizing radiation-induced changes in eye lens cell proliferation, cyclin D1 expression and lens shape. *Open Biology,* 5**,** 150011.

MORGAN, W. F. 2003. Non-targeted and delayed effects of exposure to ionizing radiation: II. Radiation-induced genomic instability and bystander effects in vivo, clastogenic factors and transgenerational effects. *Radiation Research,* 159**,** 581-596.

MORGAN, W. F. & SOWA, M. B. 2015. Non-targeted effects induced by ionizing radiation: mechanisms and potential impact on radiation induced health effects. *Cancer Lett,* 356**,** 17-21.

MOTHERSILL, C., SMITH, R. W., SAROYA, R., DENBEIGH, J., ROWE, B., BANEVICIUS, L., TIMMINS, R., MOCCIA, R. & SEYMOUR, C. B. 2010. Irradiation of rainbow trout at early life stages results in legacy effects in adults. *International Journal of Radiation Biology,* 86**,** 817-828.

NAGAMOTO, T., EGUCHI, G. & BEEBE, D. C. 2000. Alpha-smooth muscle actin expression in cultured lens epithelial cells. *Invest Ophthalmol Vis Sci,* 41**,** 1122-9.

NGUYEN, S. M., SISON, J., JONES, M., BERRY, J. L., KIM, J. W., MURPHREE, A. L., SALINAS, V., OLCH, A. J., CHANG, E. L. & WONG, K. K. 2019. Lens Dose-Response Prediction Modeling and Cataract Incidence in Patients With Retinoblastoma After Lens-Sparing or Whole-Eye Radiation Therapy. *Int J Radiat Oncol Biol Phys,* 103**,** 1143-1150.

NIETNER, T., JARUTAT, T. & MERTENS, A. 2012. Systematic comparison of tissue fixation with alternative fixatives to conventional tissue fixation with buffered formalin in a xenograft-based model. *Virchows Archiv,* 461**,** 259-269.

NOLLER, C. M., BOULINA, M., MCNAMARA, G., SZETO, A., MCCABE, P. M. & MENDEZ, A. J. 2016. A Practical Approach to Quantitative Processing and Analysis of Small Biological Structures by Fluorescent Imaging. *Journal of Biomolecular Techniques : JBT,* 27**,** 90-97.

OLSVIK, P. A., FINN, R. N., REMO, S. C., FJELLDAL, P. G., CHAUVIGNE, F., GLOVER, K. A., HANSEN, T. & WAAGBO, R. 2020. A transcriptomic analysis of diploid and triploid Atlantic salmon lenses with and without cataracts. *Exp Eye Res,* 199**,** 108150.

PAN, L., HAO, W., ZHENG, X., ZENG, X., AHMED ABBASI, A., BOLDOGH, I. & BA, X. 2017. OGG1-DNA interactions facilitate NF-κB binding to DNA targets. *Scientific Reports,* 7**,** 43297.

PARK, H.-R., JO, S.-K. & JUNG, U. 2019. Ionizing Radiation Promotes Epithelial–to–Mesenchymal Transition in Lung Epithelial Cells by TGF-β-producing M2 Macrophages. *In Vivo,* 33**,** 1773-1784.

PRAKASH, A. & DOUBLIÉ, S. 2015. Base Excision Repair in the Mitochondria. *Journal of Cellular Biochemistry,* 116**,** 1490-1499.

PUCHTLER, H. & MELOAN, S. N. 1985. On the chemistry of formaldehyde fixation and its effects on immunohistochemical reactions. *Histochemistry,* 82**,** 201-4.

RAMOS-VARA, J. A. 2005. Technical Aspects of Immunohistochemistry. *Veterinary Pathology,* 42**,** 405-426.

REMØ, S. C., HEVRØY, E. M., BRECK, O., OLSVIK, P. A. & WAAGBØ, R. 2017. Lens metabolomic profiling as a tool to understand cataractogenesis in Atlantic salmon and rainbow trout reared at optimum and high temperature. *PLOS ONE,* 12**,** e0175491.

RILEY, P. A. 1994. FREE-RADICALS IN BIOLOGY - OXIDATIVE STRESS AND THE EFFECTS OF IONIZING-RADIATION. *International Journal of Radiation Biology,* 65**,** 27-33.

SANDERSON, M. J., SMITH, I., PARKER, I. & BOOTMAN, M. D. 2014. Fluorescence Microscopy. *Cold Spring Harbor Protocols,* 2014**,** pdb.top071795-p.

SHUI, Y.-B. & BEEBE, D. C. 2008. Age-Dependent Control of Lens Growth by Hypoxia. *Investigative Opthalmology & Visual Science,* 49**,** 1023.

SHURYAK, I. 2020. Review of resistance to chronic ionizing radiation exposure under environmental conditions in multicellular organisms. *J Environ Radioact,* 212**,** 106128.

SOBOL, R. 2003. Regulated over-expression of DNA polymerase β mediates early onset cataract in mice. *DNA Repair,* 2**,** 609-622.

SONG, Y., SALBU, B., HEIER, L. S., TEIEN, H. C., LIND, O. C., OUGHTON, D., PETERSEN, K., ROSSELAND, B. O., SKIPPERUD, L. & TOLLEFSEN, K. E. 2012. Early stress responses in Atlantic salmon (Salmo salar) exposed to environmentally relevant concentrations of uranium. *Aquatic Toxicology,* 112**,** 62-71.

SYKORA, P., KANNO, S., AKBARI, M., KULIKOWICZ, T., BAPTISTE, B. A., LEANDRO, G. S., LU, H., TIAN, J., MAY, A., BECKER, K. A., CROTEAU, D. L., WILSON, D. M., SOBOL, R. W., YASUI, A. & BOHR, V. A. 2017. DNA Polymerase Beta Participates in Mitochondrial DNA Repair. *Molecular and Cellular Biology,* 37.

TEIEN, H.-C., KASHPAROVA, O., SALBU, B., LEVCHUK, S., PROTSAK, V., EIDE, D. M., JENSEN, K. A. & KASHPAROV, V. 2021. Seasonal changes in uptake and depuration of 137Cs and 90Sr in silver Prussian carp (Carassius gibelio) and common rudd (Scardinius erythrophthalmus). *Science of The Total Environment,* 786**,** 147280.

TELL, G., DAMANTE, G., CALDWELL, D. & KELLEY, M. R. 2005. The Intracellular Localization of APE1/Ref-1: More than a Passive Phenomenon? *Antioxidants & Redox Signaling,* 7**,** 367-384.

TELL, G., QUADRIFOGLIO, F., TIRIBELLI, C. & KELLEY, M. R. 2009. The Many Functions of APE1/Ref-1: Not Only a DNA Repair Enzyme. *Antioxidants & Redox Signaling,* 11**,** 601-619.

THAKUR, S., SARKAR, B., CHOLIA, R. P., GAUTAM, N., DHIMAN, M. & MANTHA, A. K. 2014. APE1/Ref-1 as an emerging therapeutic target for various human diseases: phytochemical modulation of its functions. *Experimental & Molecular Medicine,* 46**,** e106-e106.

UNSCEAR, U. N. S. C. I. T. E. O. A. R. 1993. Sources and Effects of ionizing radiation. New York.

UNSCEAR, U. N. S. C. I. T. E. O. A. R. 2008. Sources and effects of ionizing radiation *UNSCEAR 2008 report to the General Assembly with scientific annexes. Volume 2.* New York: United Nations.

UWINEZA, A., KALLIGERAKI, A. A., HAMADA, N., JARRIN, M. & QUINLAN, R. A. 2019. Cataractogenic load – A concept to study the contribution of ionizing radiation to accelerated aging in the eye lens. *Mutation Research/Reviews in Mutation Research,* 779**,** 68-81.

VASCOTTO, C., BISETTO, E., LI, M., ZEEF, L. A. H., D'AMBROSIO, C., DOMENIS, R., COMELLI, M., DELNERI, D., SCALONI, A., ALTIERI, F., MAVELLI, I., QUADRIFOGLIO, F., KELLEY, M. R. & TELL, G. 2011. Knock-in reconstitution studies reveal an unexpected role of Cys-65 in regulating APE1/Ref-1 subcellular trafficking and function. *Molecular Biology of the Cell,* 22**,** 3887-3901.

VON SALLMANN, L. 1952. Experimental studies on early lens changes after roentgen irradiation. III. Effect of x-radiation on mitotic activity and nuclear fragmentation of lens epithelium in normal and cysteine-treated rabbits. *AMA Arch Ophthalmol,* 47**,** 305-20.

WAKEFORD, R. 2004. The cancer epidemiology of radiation. *Oncogene,* 23**,** 6404-6428.

WALL, A. E. 1998. Cataracts in farmed Atlantic salmon (Salmo salar) in Ireland, Norway and Scotland from 1995 to 1997. *Vet Rec,* 142**,** 626-31.

WANG, R., HAO, W., PAN, L., BOLDOGH, I. & BA, X. 2018. The roles of base excision repair enzyme OGG1 in gene expression. *Cellular and Molecular Life Sciences,* 75**,** 3741-3750.

WATERS, J. C. 2013. Chapter 6 - Live-Cell Fluorescence Imaging. *In:* SLUDER, G. & WOLF, D. E. (eds.) *Methods in Cell Biology.* Academic Press.

WATSON, J. D., BAKER, T. A., BELL, S. P., GANN, A., LEVINE, M. & LOSICK, R. 2014. *Molecular biology of the gene. ,* Boston, Pearson Education, Inc.

WEBSTER, J. D., MILLER, M. A., DUSOLD, D. & RAMOS-VARA, J. 2009. Effects of Prolonged Formalin Fixation on Diagnostic Immunohistochemistry in Domestic Animals. *Journal of Histochemistry & Cytochemistry,* 57**,** 753-761.

WILDGOOSE, W. H. 2007. Exenteration in Fish. *Exotic DVM,* 9**,** 25-29.

WILLIAMS, D. L. 2008. Oxidative stress and the eye. *Vet Clin North Am Small Anim Pract,* 38**,** 179-92, vii.

WRIDE, M. A. 2011. Lens fibre cell differentiation and organelle loss: many paths lead to clarity. *Philos Trans R Soc Lond B Biol Sci,* 366**,** 1219-33.

WU, T.-T., CHEN, Y.-Y., CHANG, H.-Y., KUNG, Y.-H., TSENG, C.-J. & CHENG, P.-W. 2020. AKR1B1-Induced Epithelial–Mesenchymal Transition Mediated by RAGE-Oxidative Stress in Diabetic Cataract Lens. *Antioxidants,* 9**,** 273.

WU, X.-M., XI, Z.-F., LU, J., WANG, X.-Z., ZHANG, T.-Q., HUANG, X.-Y., YAO, J.-G., WANG, C., WEI, Z.-H., LUO, C.-Y., HUANG, B.-C., XU, Q.-Q., YANG, W.-P., XIA, Q. & LONG, X.-D. 2017. Genetic Single Nucleotide Polymorphisms (GSNPs) in the DNA Repair Genes and Hepatocellular Carcinoma Related to Aflatoxin B1 among Guangxiese Population. *Genetic Polymorphisms.* InTech.

XANTHOUDAKIS, S., MIAO, G. G. & CURRAN, T. 1994. The redox and DNA-repair activities of Ref-1 are encoded by nonoverlapping domains. *Proceedings of the National Academy of Sciences,* 91**,** 23-27.

XU, B., KANG, L., ZHANG, G., WU, J., ZHU, R., YANG, M. & GUAN, H. 2015. The Changes of 8-OHdG, hOGG1, APE1 and Pol β in Lenses of Patients with Age-Related Cataract. *Current Eye Research,* 40**,** 378-385.

YOULE, R. J. & NARENDRA, D. P. 2011. Mechanisms of mitophagy. *Nature Reviews Molecular Cell Biology,* 12**,** 9-14.

ZHANG, L., WANG, Y., LI, W., TSONIS, P. A., LI, Z., XIE, L. & HUANG, Y. 2017. MicroRNA-30a Regulation of Epithelial-Mesenchymal Transition in Diabetic Cataracts Through Targeting SNAI1. *Scientific Reports,* 7.

ZHAO, H., CHEN, Y., REZABKOVA, L., WU, Z., WISTOW, G. & SCHUCK, P. 2014. Solution properties of γ-crystallins: Hydration of fish and mammal γ-crystallins. *Protein Science,* 23**,** 88-99.

ZHOU, R., SI, J., ZHANG, H., WANG, Z., LI, J., ZHOU, X., GAN, L. & LIU, Y. 2014. The effects of x-ray radiation on the eye development of zebrafish. *Human & Experimental Toxicology,* 33**,** 1040-1050.

Appendix A:

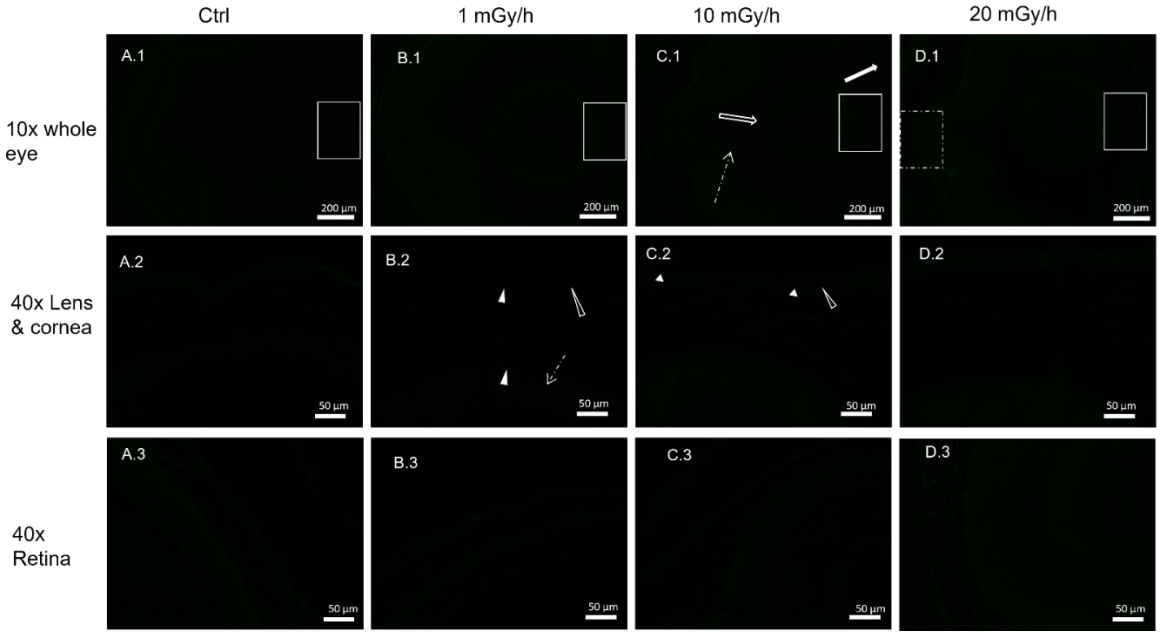

Figure A.1. Representative immunofluorescent images of LC3 stained samples. The left column is 10x magnification of eye, the middle is 40x magnification of lens and cornea and the left column is 40x magnification of the retina. These images are from the green channel and are complimentary to the images from the red channel. The brightness have been increased in software in parallel with the red channel images to serve as a reference making sure that the signal seen in the rhodamine(red) channel is not due to autofluorescence.

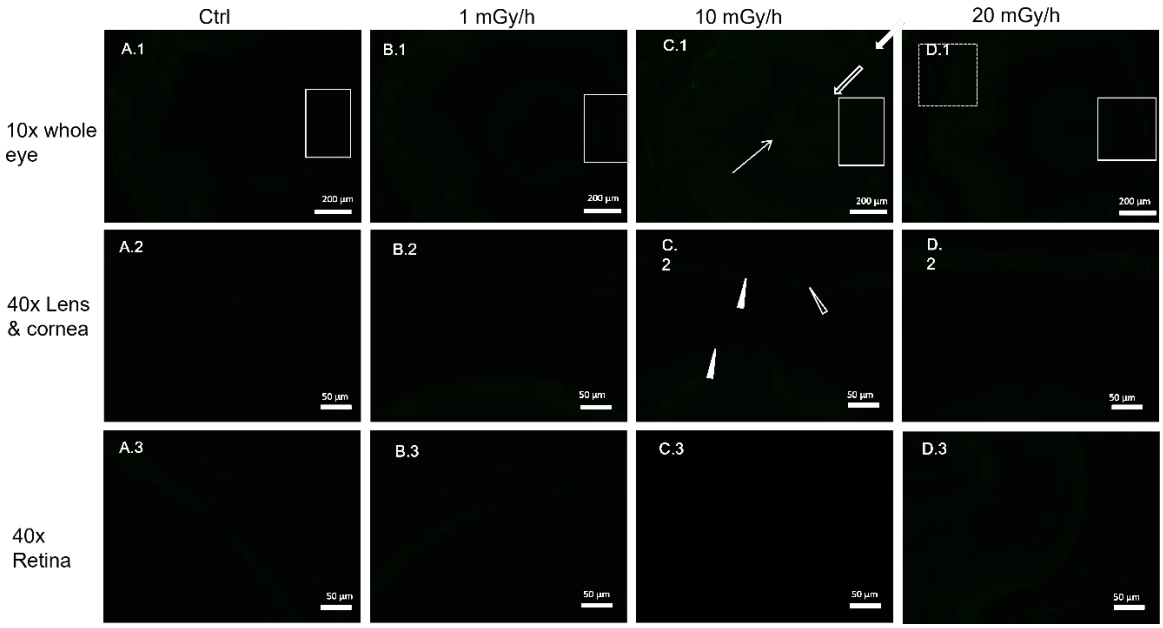

Figure A.2. Representative immunofluorescent images of OGG1 labeled samples. The left column is 10x magnification of eye, the middle is 40x magnification of lens and cornea and the left column is 40x magnification of the retina. These images are from the green channel and are complimentary to the images from the red channel. The brightness have been increased in software in parallel with the red channel images to serve as a reference making sure that the signal seen in the rhodamine(red) channel is not due to autofluorescence.

Appendix B:

Table B.1. Summary of tissue processing program used by the Tissue-Tek®. VIP™ 5 Jr (Sakura Finetek, USA).

Step	*Solute*	*Time (min)*	*Temperature (°C)*
1	70% EtOH	15	35
2	80% EtOH	15	35
3	90% EtOH	15	35
4	100%EtOH	30	35
5	100%EtOH	30	35
6	100%EtOH	60	35
7	Xylene	30	35
8	Xylene	30	45
9	Xylene	30	50
10	Paraffin	60	58
11	Paraffin	60	58
12	Paraffin	60	58
13	Paraffin	60	58

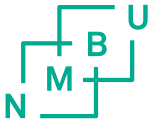

Norges miljø- og biovitenskapelige universitet
Noregs miljø- og biovitskapelege universitet
Norwegian University of Life Sciences

Postboks 5003
NO-1432 Ås
Norway